TRIBHUVAN UNIVERSITY

INSTITUTE OF ENGINEERING

PULCHOWK CAMPUS

THESIS NO.: M-343-MSREE-2020-2022

Flow Analysis in Asymmetric and Symmetric Bifurcation with Varied Layout: A Case Study of Daram Khola HEP

by

Prashant Neupane

A THESIS

SUBMITTED TO THE DEPARTMENT OF MECHANICAL AND AEROSPACE ENGINEERING

IN THE PARTIAL FULFILMENT OF THE REQUIREMENTS

FOR THE DEGREE OF MASTERS OF SCIENCE IN

RENEWABLE ENERGY ENGINEERING

DEPARTMENT OF MECHANICAL AND AEROSPACE ENGINEERING

LALITPUR, NEPAL

September, 2022

COPYRIGHT

TRIBHUVAN UNIVERSITY

INSTITUTE OF ENGINEERING

PULCHOWK CAMPUS

DEPARTMENT OF MECHANICAL AND AEROSPACE ENGINEERING

The undersigned certify that they have read and recommended to the Institute of Engineering for acceptance, a thesis entitled "**Flow Analysis in Asymmetric and Symmetric Bifurcation with Varied Layout: A Case Study of Daram Khola HEP**" submitted by Prashant Neupane in partial fulfillment of the requirements for the degree of Masters of Science in Renewable Energy Engineering.

_____

Supervisor, Dr. Mahesh Chandra Luintel

Professor, Department of Mechanical and Aerospace Engineering, Pulchowk Campus

_____

External Examiner, Er. Dipesh Thapa

CEO, TAC Hydro Consultancy Pvt.ltd

_____

Committee Chairperson, Assoc. Prof. Dr. Surya Prasad Adhikari

Head, Department of Mechanical and Aerospace Engineering

Pulchowk Campus

Dare: 2079/06/02

ABSTRACT

A bifurcation is used whenever it is needed to divide the fluid flow into more than one turbines for power generation, taking the water from a single reservoir or head works. Bifurcation is one of the critical parts of a hydropower project which contributes to head loss in the penstock manifold. The design and layout of a bifurcation are determined by the available head of water, flow rate, geological constraints and fabrication and economic constraints. The design of a bifurcation can be done conventionally using analytical techniques, design codes and guidelines. Nowadays with the advancement of computing devices, computational methods along with relevant software applications can be used for the design process for more accurate results. In this study, a case of Daram Khola HPP has been considered where the layout of bifurcation is mainly constrained by the geological arrangement that are the axis of penstock pipe, axes of the two turbine inlets and the center to center distance between the two turbine inlets. First, an asymmetric bifurcation layout is developed which is modeled and analyzed to determine head loss and flow distribution pattern in the two branch pipes. Modeling is done in ANSYS SpaceClaim and fluid flow analysis incorporating Computational Fluid Dynamics is carried out in ANSYS Fluent. The asymmetric layout is revised by changing the angle of bifurcation to 45° and similar analysis are performed. These layouts are further revised by incorporating symmetric bifurcation with angle of bifurcation 60° and adding a bend pipe just upstream of the bifurcation. Multiple layouts are proposed with change in upstream bend angle by 1° in each revision, ranging the bend angle from 24° to 32°. Flow simulation, analysis and head loss calculation is done for each layout and the results are compared. The difference in mass flow rate at the two outlets has decreased from 829.83 kg/s in the asymmetrical layout to 140.82 kg/s in the symmetric layout with bend angle 31°. The head loss in outlet 1 and outlet 2 of the asymmetrical layout are 214.70 mm and 624.38 mm respectively, while for the symmetric layout, the head loss is minimum for outlet 1 at a bend angle of 32° i.e. 223.30 mm and for outlet 2 at 24° i.e. 171.08 mm. Since the mass flow rate difference in the two outlets is minimum for bend angle 31° and head loss in the two outlets are also close to the lowest head loss for each outlets in the considered range, it is concluded to be the optimum layout.

ACKNOWLEDGEMENTS

I would like to express my deepest gratitude and sincere thanks to my thesis supervisor Prof. Dr. Mahesh Chandra Luintel for his expert guidance, constant support and suggestion whenever required and continuous encouragement throughout the research period.

I would also like to express my sincere appreciation to the Department of Mechanical and Aerospace Engineering and Institute of Engineering for their support to the thesis. My appreciation extended to Dr. Surya Prasad Adhikari, Head of Department of Mechanical and Aerospace Engineering, Pulchowk Campus for his co-operation and guidance. I would like to express my sincere gratitude and thanks to Dr. Hari Bahadur Darlami, program coordinator, MSREE, for providing a good interactive environment for thesis work and also to the entire elite committee members for valuable comments and recommendations for making this work more meaningful.

Finally, I would like to convey my sincere thanks to my colleagues of 076MSREE as well as my family members for their support, encouragement and constant source of inspiration during the entire period of thesis work.

TABLE OF CONTENTS

LIST OF FIGURES

LIST OF TABLES

LIST OF ABBREBATIONS

2D	: Two Dimensional
3D	: Three Dimensional
CAD	: Computer Aided Drawing
CFD	: Computational Fluid Dynamics
DNS	: Direct Numerical Simulation
FEM	: Finite Element Method
HDPE	: High Density Polyethylene
HEP	: Hydro-Electric Project
LES	: Large Eddy Simulation
MW	: Megawatts
PROR	: Peaking Run-Off-River
RANS	: Reynolds Averaged Navier-Stokes Simulation
ROR	: Run-Off-River
SIMPLE	: Semi Implicit Method for Pressure Linked Equations
SRS	: Scale Resolving Simulation
SST	: Shear Stress Transport

CHAPTER ONE: INTRODUCTION

1.1 Background

A Penstock can be defined as a pressurized water conduit that carries water under pressure to the turbine of a hydropower plant from a free water surface. The free water surface may be either surge chamber, reservoir or a Forebay. The penstocks should be hydraulically efficient as much as practical to conserve available head and also structurally safe to prevent failure under varied conditions (AEPC, 2014).

These penstock pipes are mostly made up of welded carbon steel. HDPE pipes can also be used if the size of penstock and the head of water available is small. The size of penstocks is a tradeoff between the head loss incurring in the pipes and the material requirement (Thapa et al., 2016).

The turbines and generators of a hydropower plant needs periodic repair and maintenance and if only a single generating unit is available, the power generation will be lost during the shutdown time required for maintenance works. Hence, most of the plants are designed with at least two generating units. Also, the flow rate of water available for the power plant varies significantly according to the season in case of ROR or PROR type hydropower plants, especially in context of Nepal (NEA, 2020). Operating the turbine with discharge significantly lower than design discharge results in low efficiency (Rajput, 1998)

Hence, using more than one generating units is a common practice and each one of them will be required to be supplied with water through penstock. Using separate penstock to feed each generating unit is not economically and sometimes geographically justified. For this purpose, a single penstock is used to transport water from free water surface to the powerhouse location. The penstock is then branched depending upon the number of turbines, each branch feeding a single unit. In the case where the number of units is two, the penstock pipe is branched into two equal halves and such branching is called the penstock bifurcation (Thapa et al., 2016).

Bifurcation is one of the critical parts of a hydropower project which contributes to head loss in the penstock manifold. The water flow pattern inside a bifurcation is complex due to geometries with varied cross sections and sudden change in flow direction. The behavior of water in such complexities cannot be easily predicted. Hence, special care and design considerations are required both hydraulically and structurally while working with a bifurcation (Koirala et al., 2017). The design and layout of a bifurcation are determined by the available head of water, flow rate, geological constraints and fabrication and economic constraints.

Due to obstruction in flow and the change in flow direction, a considerable amount of head loss occurs in the bifurcation which decreases the net head available at the turbine inlet. The hydraulic optimization should be done regarding the pressure or head loss in the bifurcation which should be under 2% of the total pressure head at the inlet (Parajuli et al., 2021). Determination of such head loss by analytical methods is a tedious task. Although some empirical relations are available in the design codes in the form of head loss coefficients, they are applicable only on selected geometries having pre-specified values of angle of bifurcation. Hence, for analyzing the flow and determining the head loss along a bifurcation layout, Computational Fluid Dynamics (CFD) approach of problem solution is a suitable method and is the current industrial practice.

The CFD approach can also be utilized to determine the distribution of flow in the two branches (Kandel & Luitel, 2019). It is an important parameter because the distribution is desired to be equal in the two branches in most of the cases, as the two generating units are mostly of same rating.

The bends present in the penstock pipe accounts for minor head losses. Hence, head loss due to obstruction of flow and change in flow direction, head loss due to bends and head loss due to wall friction all contributes to the total head loss in the bifurcation layout arrangement (Ahmed, 1965).

1.2 Problem Statement

Due to the complex structure of bifurcation and due to inherent fluid and material characteristics, the bifurcation is one of the major areas of head loss along the penstock conduit. The layout of the bifurcation arrangement, along with the shape of bifurcation impacts the overall performance of the bifurcation system. In the case considered, using symmetric bifurcation without changing the axis of penstock pipe is not possible due to constraints imposed by civil layout and the power house orientation. Using an asymmetric bifurcation may result in larger head loss or unequal distribution of flow. A bend can be introduced just upstream of the bifurcation to deviate the flow such that a symmetric bifurcation can be used conforming to the site constraints. This study aims to perform analysis on such asymmetric and symmetric cases and explore the relation of the flow distribution and head loss with the change in upstream bend angle and subsequent geometrical changes incurred by it.

1.3 Objectives

1.3.1 Main Objective

The main objective of this study is to perform flow analysis and compare head loss and flow distribution of asymmetric and symmetric bifurcation layout with varying bend angle just upstream of the bifurcation.

1.3.2 Specific Objectives

The specific objectives of this thesis are,

i) To conduct CFD analysis of asymmetric bifurcation and symmetric bifurcation layout.

ii) To successively revise the symmetric bifurcation layout and perform CFD analysis on them.

iii) To visualize pressure field and velocity field for each layout.

iv) To determine head loss and flow distribution for each layout.

1.4 Assumptions and Limitations

i) Water is considered as an incompressible fluid.

ii) Provision of sickle plate is not incorporated.

iii) The geometry of symmetric bifurcation is kept unvaried while changing the bend angles.

iv) Pressure is assumed to be constant and equal to 1 atmospheric pressure at both outlets.

CHAPTER TWO: LITERATURE REVIEW

2.1 Bifurcation

Bifurcation of Penstock in the Hydropower plant is used to divide the flow into the two turbine units for power generation. This division can be either symmetric or asymmetric. The symmetric bifurcation refers to such arrangement where the two branches of bifurcation are symmetric about the axis of the main inlet pipe and asymmetric refers to such arrangement where the branches are not symmetric. The flow distribution is usually equal in both the branches in case of symmetric bifurcation if it is not altered by other manifold conditions. They are usually installed near the powerhouse where the maximum possible pressure prevails i.e. the static pressure and the surge pressure, which have an extra ordinary hydraulic and mechanical behavior related to vibration, power swings, propagation of pressure, hence both the considerations are important. (Koirala et al., 2017)

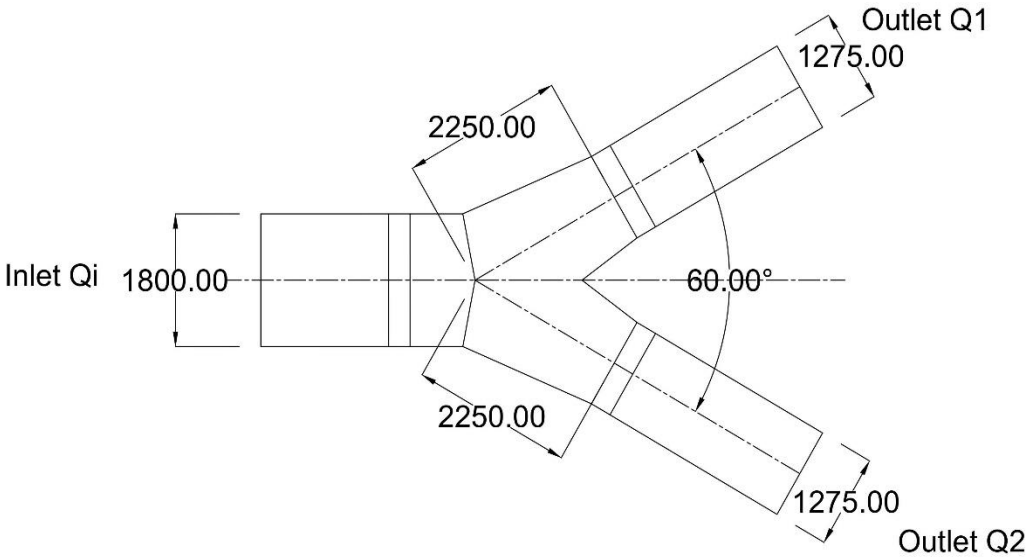

Figure 2. 1: Sample drawing of a bifurcation

2.2 Hydraulic Considerations for Flow of Water through Bifurcation

While designing the branch, the following hydraulic considerations should be taken care of, during pressure flow conditions (BIS, 2009):

a) Head loss due to branch should be small.

b) The total head loss in the penstock before and after the branching should be small.

c) Turbulent and secondary flows should not be allowed to be generated.

d) For equi-branch, head loss in each pipe should be of similar value.

e) In case the flow rate in one branch pipe changes, a large vortex or a hydraulic pulsation should not take place in the flow of the other branch pipes.

2.3 Governing Equations of Fluid Flow

Generally, fluid flow problems for viscous conditions are studied by using three fundamental equations. These equations are based on the conservation of physical systems as explained in this section. (Anderson, 1992)

1. Mass conservation equation (continuity equation)

$$\frac{\partial \rho}{\partial t} + \nabla \cdot (\rho \vec{V}) = 0 \qquad \text{Equation 2.1}$$

2. Momentum conservation equation (Newton's second law)

$$\frac{\partial(\rho u)}{\partial t} + \nabla \cdot (\rho u \vec{V}) = -\frac{\partial p}{\partial x} + \frac{\partial \tau_{xx}}{\partial x} + \frac{\partial \tau_{yx}}{\partial y} + \frac{\partial \tau_{zx}}{\partial z} + \rho f_x \qquad \text{Equation 2.2(a)}$$

$$\frac{\partial(\rho v)}{\partial t} + \nabla \cdot (\rho v \vec{V}) = -\frac{\partial p}{\partial y} + \frac{\partial \tau_{xy}}{\partial x} + \frac{\partial \tau_{yy}}{\partial y} + \frac{\partial \tau_{zy}}{\partial z} + \rho f_y \qquad \text{Equation 2.2(b)}$$

$$\frac{\partial(\rho w)}{\partial t} + \nabla \cdot (\rho w \vec{V}) = -\frac{\partial p}{\partial z} + \frac{\partial \tau_{xz}}{\partial x} + \frac{\partial \tau_{yz}}{\partial y} + \frac{\partial \tau_{zz}}{\partial z} + \rho f_z \qquad \text{Equation 2.2(c)}$$

When equations of stress are substituted to the equation of momentum for common Newtonian fluids, in the Equation 2.2, it gives the Navier-Stokes equation which is fundamental equation of fluid flow in partial form.

3. Energy conservation equation (first law of thermodynamics)

$$\rho\,(Dh/Dt) = (Dp/\,Dt) + \nabla\,(k\nabla T) + \Phi \qquad \text{Equation 2.3}$$

Where, Φ is known as dissipation function, is given by,

$$\Phi = \tau_{ij}{}'\,(u_i/x_j)$$

The involved viscous stress tensor $\tau_{ij}{}'$ is obtained by,

$$\tau_{ij}{}' = \mu\,(\partial u_i/\partial x_j + \partial u_j/\partial x_i) + \delta_{ij}\lambda\,(\nabla \cdot \mathbf{V}) \qquad \text{Equation 2.4}$$

In this research, the numerical simulation assumes that the fluid involved is incompressible (density is constant). Rewriting the continuity equation for incompressible ($\rho = constant$) flow, we have,

$$\nabla \cdot \vec{V} = 0 \qquad \text{Equation 2.5}$$

Here the effect of temperature is neglected so, Equation 2.3 is not taken into account.

2.4 Head Loss in Bifurcation

The head loss in a bifurcation due to branching, ΔH, can be expressed as shown in the equation 2.6.

$$\Delta H = \alpha \frac{V_0^2}{2g} \qquad \text{Equation 2.6}$$

Where,

V_o = mean velocity of flow in the main pipe,

α = head loss coefficient.

Value of α is influenced by the branch angle, change in the sectional area, distribution ratio of the flow to each branch pipe, and the Reynolds's Number. An estimation of the head loss coefficient for different branch angles can be made from Figure 2.2, while influence

of Reynolds's number of main pipe over the head loss coefficient, in case of conical wye having equal distribution amongst the branches, is given at Figure 2.3. (BIS, 2009)

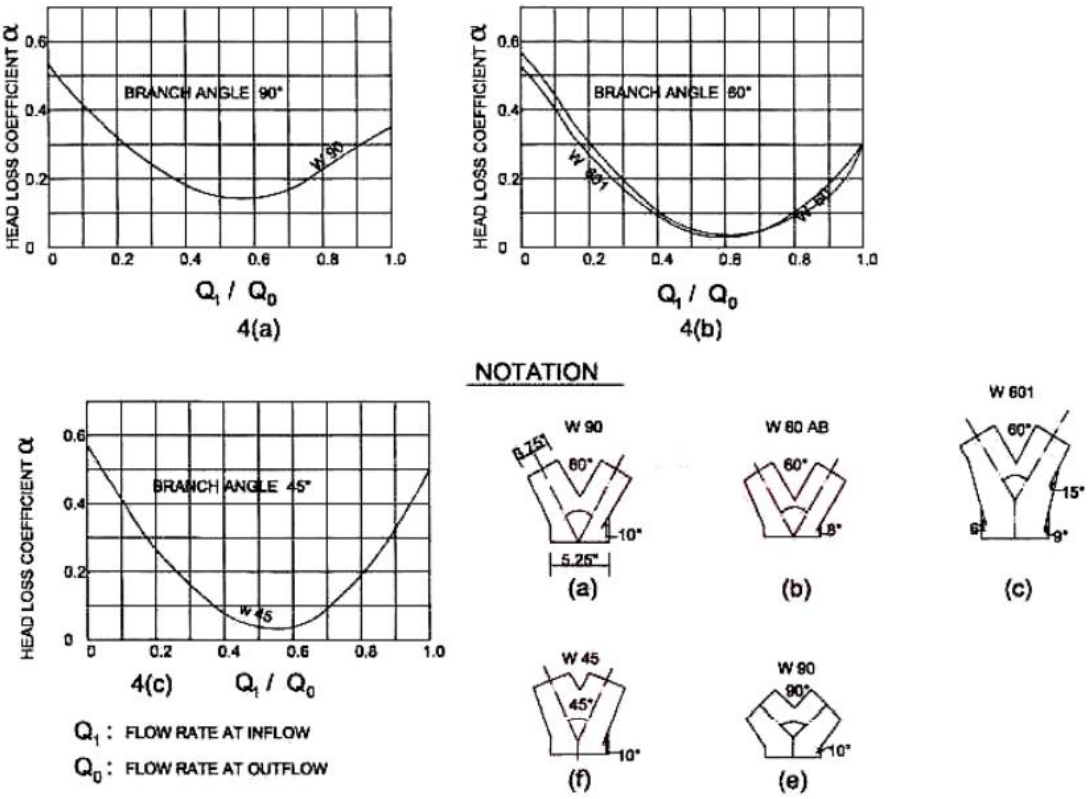

Figure 2. 2: Head Loss Coefficient for different branch angles

Source: BIS. (2009). *Penstock Branch Design Manual* (Vol. 14, Issue November)

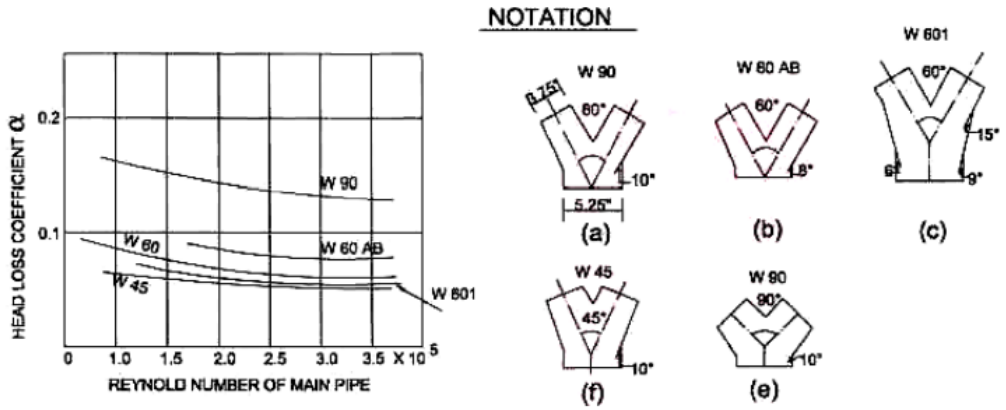

Figure 2. 3: Head loss coefficient for different Reynolds number

Source: BIS. (2009). *Penstock Branch Design Manual* (Vol. 14, Issue November)

Angle of bifurcation, ratio of cross sectional area, type and shape of bifurcation, flow, velocity and Reynolds's number are some of the major factors governing head losses (Koirala et al., 2017). Approximation of these parameters using set of equations at two dimensions may not be relevant to determine the effectiveness. So far the practices are concerned, often hydraulic design (angle) of bifurcation are prepared based on the flow ratio referencing the graphs resulted from various researches. In some cases the graph may give a valid bifurcation angle (but it's rare the cases match) but many others were designed on larger hydraulic losses. Graphical representation from the Miller experiments and Munich test are some of the major representations. Fig 2.4 shows the representation from Miller's experiment (Miller, 1990)

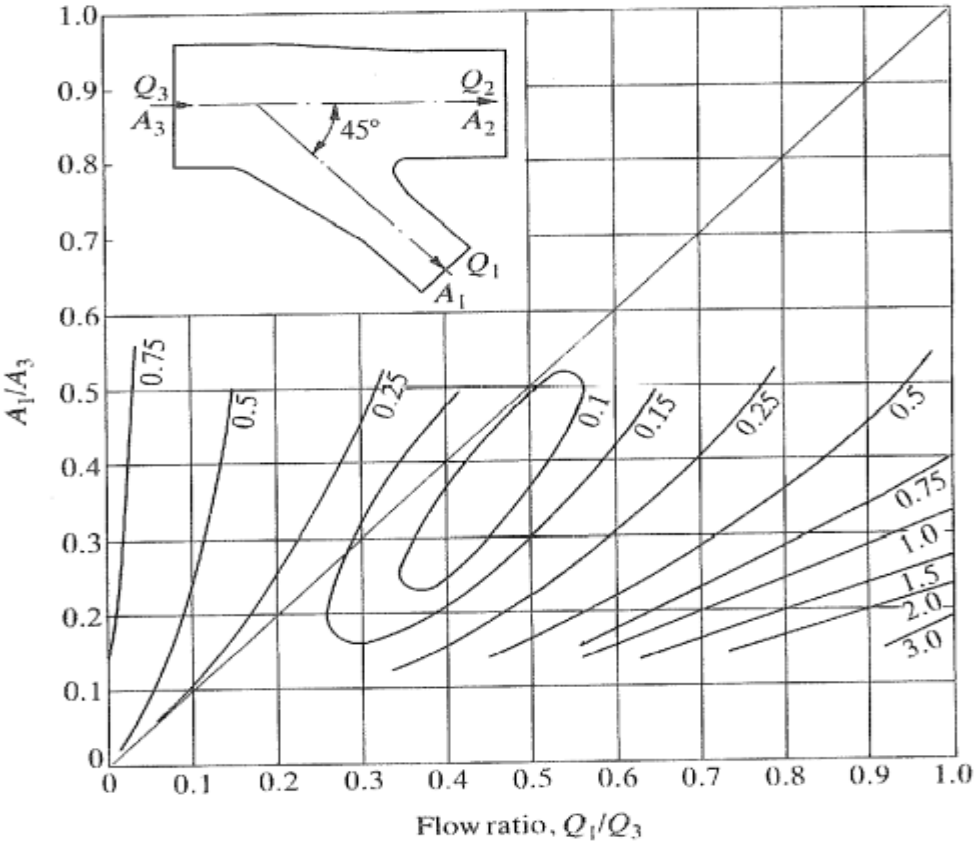

Figure 2. 4: Miller's Plot for Head Loss Coefficient in Bifurcation

(Source: Internal Flow Systems 2nd Edition, D.S. Miller)

Here, the head loss coefficient is plotted as a function of the ratio of area of inlet pipe and branch pipe (A_1/A_3) and the ratio of flow rate in the inlet pipe and the branch pipe (Q_1/Q_3) for a specified angle of bifurcation of 45°.

While determining the head loss in a bifurcation layout, the loss due to the bends in the branch pipe must also be considered. Moreover, the friction loss on the whole of the layout pipes also contributes to total head loss. The head loss due to bends in a circular pipe system is given by the equation 2.7(Miller, 1990).

$$\Delta H = K_b \frac{U^2}{2g} \qquad \text{Equation 2.7}$$

Where,

U = inlet velocity

K_b = bend head loss coefficient

Values of K_b mainly depends upon the angle of bend (θ) and the ratio of bend radius and the pipe diameter (r/d). The variation of K_b with the mentioned parameters is shown graphically is figure 2.5.

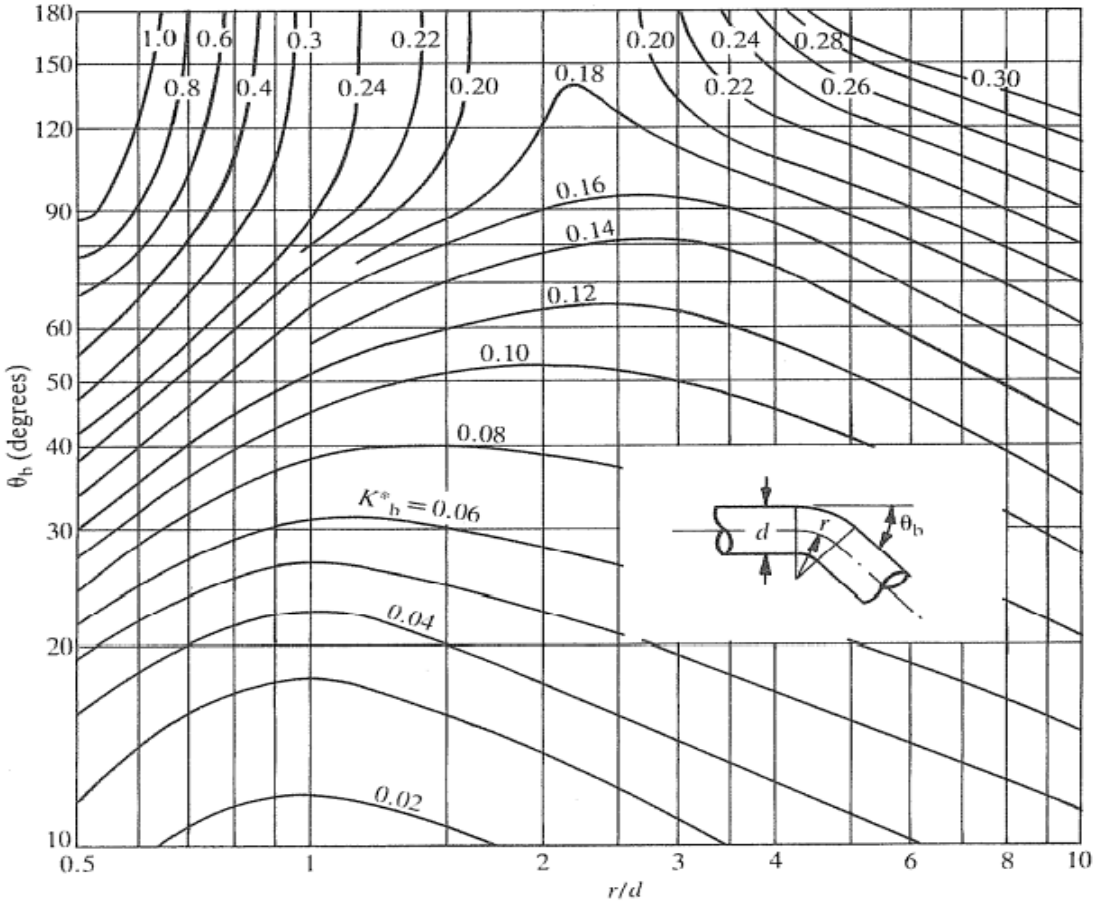

Figure 2. 5 Head loss Coefficient for bends

(Source: Internal Flow Systems 2nd Edition, D.S. Miller)

The friction loss in the pipes involved in the manifold can be determined by using the Darcy-Weisbach formula given by equation 2.8(Rajput, 1998).

$$h_f = \frac{4fLV^2}{2gD} \qquad \text{Equation 2.8}$$

Where,

h_f = Loss of head due to friction

f = Co-efficient of friction (a function of Reynolds number, Re)

L = Length of the pipe

V = Mean velocity of flow, and

D = Diameter of the pipe.

The coefficient of friction can be determined with the help of Moody Diagram.

The available plots, graphs and codes are useful in determining head loss and flow behavior in bifurcations of simple geometry and layouts only. For cases of asymmetric bifurcations and other variations in the bifurcation layout, mathematical modeling and empirical relations are not much useful. Hence, a computational method can be utilized to determine the flow behavior in such complex cases (Sukhapure et al., 2017). Computational Fluid Dynamics (CFD) can model the flow conditions and best determine the flow behavior when provided with appropriate boundary conditions (Versteeg & Malalasekera, 2005).

2.5 Use of CFD in flow analysis

The flow through a straight penstock pipe under pressure is relatively simple and can be represented by the one dimensional and two dimensional flow equations. Whereas, the flow involving a bifurcation is complex near and difficult to be represented by the closed form mathematical solution. For such cases, model analysis or the Computational fluid dynamics (CFD) can describe the flow pattern and provide appropriate results (Dhungana, 2020). Finite element method of discretization divides the fluid domain into a number of discrete subdomains (elements, control volumes etc.) of tetrahedral or hexahedral elements. Each subdomain is represented by a discrete set of points (nodes or grid points). The flow parameters are assigned to each node. The nodal parameters known at the boundary are known as a boundary conditions. The governing differential equations are converted into a

system of algebraic equations valid at each of these discrete points. The coefficient matrix of the linear equations of each element is formed which is known as the element stiffness matrix. These matrixes of all elements are combined together forming global stiffness matrix. The global stiffness matrix is solved to obtain the relevant parameters at each node. Different CFD tools are available to perform these tasks in an efficient manner. ANSYS CFX and FLUENT are the popular CFD tools for modeling of flow provided with appropriate boundary conditions (Thapa et al., 2016).

2.5.1 Turbulence Modeling

The flow which follows a predefined streamline throughout the analysis for a specific time period, it is known as laminar flow. When in that certain flow the parameter values starts to increase and it attains highly disturbed flow regime throughout the analysis time, it is known as turbulent flow.

Turbulent flow is highly irregular and non-linear with high dissipation of energy and diffusivity forming vortex. Whenever a study of highly turbulent flow is required, it is followed by a rigorous approach with involvement of complex parameters and processes (Dhungana, 2020)

Laminar and turbulent flow is characterized by the study of Reynold's Number, which is defined as the ratio of inertial force to the viscous force. Whenever its value is higher, that means inertial force overcomes the viscous force disturbances and disorder occurs known as turbulence. Reynolds' Number is defined mathematically as,

$$\text{Reynolds Number} = \frac{Inertial\ Force}{Viscous\ Force} = \frac{\rho VL}{\mu} \qquad \text{Equation 2.9}$$

Where, ρ is the fluid density

V is the velocity of fluid

L is the characteristic length which is equal to the pipe diameter in case of pipe flow

μ is the dynamic viscosity of fluid

In real field, all the fluid flow which are to be studied in an engineering design or research are almost turbulent. Among several techniques for solving the turbulence model, Direct

Numerical Simulation (DNS) numerically solves the governing equation of the fluid flow: Navier-Stokes equations. It does not require any model and has high computational cost. Scale Resolving Simulation (SRS) which includes Large Eddy Simulation (LES) resolves the motion of largest eddies in the calculation and smaller eddies than the mesh is modeled. It is an inherently unsteady method as it generates long run times and large volume data due to small time steps and requires higher grid resolution. Reynolds Averaged Navier-Stokes Simulations (RANS) is most used and appropriate approach for pipe flow simulations. DNS and SRS are more demanding and complex for the problem herein.

Reynolds Averaged Navier-Stokes (RANS)

RANS model solves the Reynolds averaged Navier-Stokes equations in a time averaged framework in which steady state solution are possible. It models all turbulence including the large eddies. For the analysis of flows in an industrial application, it plays a vital role and it is also extensively used for conducting analysis of turbulent flow with steady state approach. To represent the highly turbulent fluctuations, mean value of the flow quantities are used by the equations in this approach. It is also called Statistical Turbulence Model due to its nature of using statistical averaging procedure.

K-ε Turbulence Model

It is well-known and often used in industry. With this model, the turbulent flow is characterized by 3 mean fields: the mean velocity *v*, the turbulence kinetic energy *k* and the dissipation rate ε. This model is valid in turbulent areas (Gisselbrecht & Plaut, 2017).

The standard k–ε model has two model equations, one for k and one for ε, based on the best understanding of the relevant processes causing changes to these variables (Versteeg & Malalasekera, 2005). k and ε are used to define velocity scale *v* and length scale *l* representative of the large-scale turbulence as follows:

$$v = k^{1/2} \quad , \quad l = \frac{k^{3/2}}{\varepsilon} \qquad \text{Equation 2.10}$$

The standard k–ε model uses the transport equations for k and ε shown in equation 2.11 and equation 2.12.

$$\frac{\partial(\rho k)}{\partial t} + \nabla(\rho U k) = \nabla\left[\left(\mu + \frac{\mu_t}{\sigma_k}\right)\nabla k\right] + P_k + P_b - \rho\varepsilon + S_k \qquad \text{Equation 2.11}$$

$$\frac{\partial(\rho\varepsilon)}{\partial t} + \nabla(\rho U \varepsilon) = \nabla\left[\left(\mu + \frac{\mu_t}{\sigma_\varepsilon}\right)\nabla\varepsilon\right] + C_1\frac{\varepsilon}{k}(P_k + C_3 P_b) - C_2\,\rho\frac{\varepsilon^2}{k} + S_\varepsilon$$

Equation 2.12

Where,

P_k = production due to mean velocity shear

P_b = production due to buoyancy

S_k = user defined source

Two partial differential equations (transport equations) are solved in this type of turbulence model: the turbulent kinetic energy k and the turbulence eddy dissipation ε (i.e., the rate at which the turbulent kinetic energy dissipates) (Shaheed et al., 2019).

It is usually useful for free-shear layer flows with relatively small pressure gradients as well as in confined flows where the Reynolds shear stresses are most important. It can also be stated as the simplest turbulence model for which only initial and/or boundary conditions needs to be supplied. Hence, it is less computationally expensive and properly model the flow in free stream region. For flow near the walls, standard wall functions with fine meshing provided by inflation layers can compensate for the drawbacks.

2.5.2 Meshing

Meshing is the process in which the continuous geometric space of an object is broken down into thousands or more of shapes to properly define the physical shape of the object. This process typically consumes a significant portion of the time in acquiring simulation results. ANSYS Meshing provides advanced automated mesh generation tools can provide faster and more accurate solutions for CFD Meshing(ANSYS Inc, 2016).

Meshing, also known as mesh generation, is the process of generating a two-dimensional and three-dimensional grid; it is dividing complex geometries into elements that can be used to discretize a domain.

Meshing has a significant role when it comes to the engineering simulation process. Creating a high-quality mesh is one of the most critical factors that should be considered to ensure simulation accuracy.

Creating the most appropriate mesh is the foundation of engineering simulations because the mesh influences the accuracy, convergence, and speed of the simulation. Computers cannot solve simulations on the CAD model's actual geometry shape as the governing equations cannot be applied to an arbitrary shape.

Mesh elements allow governing equations to be solved on predictably shaped and mathematically defined volumes. Typically, the equations solved on these meshes are partial differential equations.

Due to the iterative nature of these calculations, obtaining a solution to these equations is not practical by hand, and so computational methods such as Computational Fluid Dynamics (CFD) and Finite Element Analysis (FEA) are employed.

Body sizing, inflation layers, sphere of influence, meshing methods are some important factors to be considered while generating a good quality mesh. The quality of mesh can be monitored by mesh skewness, orthogonal quality, aspect ratio and many other mesh metrics.

2.6 Related Works

The major extensive study on bifurcation are focused on structural geometry of the bifurcation considering the branch angles to minimize the head loss. Some are also focused on the comparison of two successive bifurcations against a single trifurcation in case of three generating units.

Thapa et al., 2016 has applied CFD and FEM for the design and analysis of penstock bifurcation. The setup of Kulekhani-III Hydropower Project has been chosen for the study. Flow analysis was carried out on the proposed manifold arrangement after modeling. The head loss was calculated and the manifold was revised consecutively to determine a geometry with most efficient performance. The thickness and reinforcements required for the bifurcation was calculated and the solid model was subjected to Finite Element Analysis. The loss coefficient was reduced from 0.44 to 0.21 (Thapa et al., 2016).

Hanumanthappa et al., 2010 has discussed the hydrostatic test conducted on penstock bifurcation of Varahi Hydro Electric (430MW) project, Karnataka by measuring strains at seventeen pre-selected critical locations. Critical locations were selected on the outer surface of the penstock bifurcation and on the surface of sickle plate inside the bifurcation at which the rosette, biaxial and uniaxial strain gauges were installed. (Hanumanthappa et al., 2010)

Koirala et al., 2017 identified the multi prospect approach for design of Bifurcation, incorporating the modern day's tools and technology. A computational design of bifurcation was performed by taking a case study of Darundi Khola Hydropower Project. The structural members were designed incorporating both the analytical method and the finite element method. Analytical calculations were used for pre-estimation while the finite element was used for optimized solution (Koirala et al., 2017).

A computational research has been carried out by Kandel & Luitel, 2019, to determine the most efficient branching method for a manifold which has three generating units. The case of Solukhola-Dudhkoshi Hydropower Project, having three units of turbines was chosen for the study. Various models were prepared and flow pattern was visualize, to determine a setup with minimum loss of head and mas flow variation in the 3 different outlets. The research finally concluded that a single trifurcation performed better compared to two successive bifurcations or three parallel branching form main pipe (Kandel & Luitel, 2019).

Aguirre & Camacho, 1967 has performed head losses analysis in symmetrical trifurcations of penstocks in high pressure pipeline systems using CFD. This study has focused on the quantified losses as a function of the volumetric flow rate, using computational fluid dynamics (CFD). To determine the coefficient of losses three mesh settings were analyzed: hexahedral, tetrahedral and hybrid, considering steady state flow. The k-ω turbulence model is used, with refinement near wall elements, quantified the y plus. Results of loss coefficients for different volumetric flow rate and different mesh discretization method are evaluated and compared (Aguirre & Camacho, 2014).

Dangi et al., 2022, performed numerical analysis in manifold of Phukot Karnali Hydroelectric Project. Initially, branching angle in the manifold was designed to be 45°. Numerical analysis was done on ANSYS platform by changing branching angle in both

forward and backward direction at the interval of 10°. Head loss was computed to be minimum for 30°. In addition, cone length was also changed and analysis were performed with and without sickle plate. The optimized profile was created by combining best branch angle, best cone length and sickle plate. The head loss at outlet-1, outlet-2 and outlet-3 for the optimized profile were computed as 0.13m, 0.46m and 0.31m, respectively. When head loss at three sections in optimized case and base case were compared, it was found that head loss for optimized case at outlet-1, outlet-2 and outlet-3 were 37%, 15% and 24% less as compared to the base case (Dangi et al., 2022).

R. Saheed and H. Gildeh compared the performance of standard k-ε and realizable k-ε turbulence model in curved and confluent channels to conclude that standard k-ε performed better in the curved channel and the realizable k-ε model performed better in the confluent channel (Shaheed et al., 2019).

CHAPTER THREE: METHODOLOGY

3.1 General Methodology

The flow distribution comparison and head loss comparison of asymmetric bifurcation and symmetric bifurcations with varied layout was carried out in the steps as described in the flow chart below:

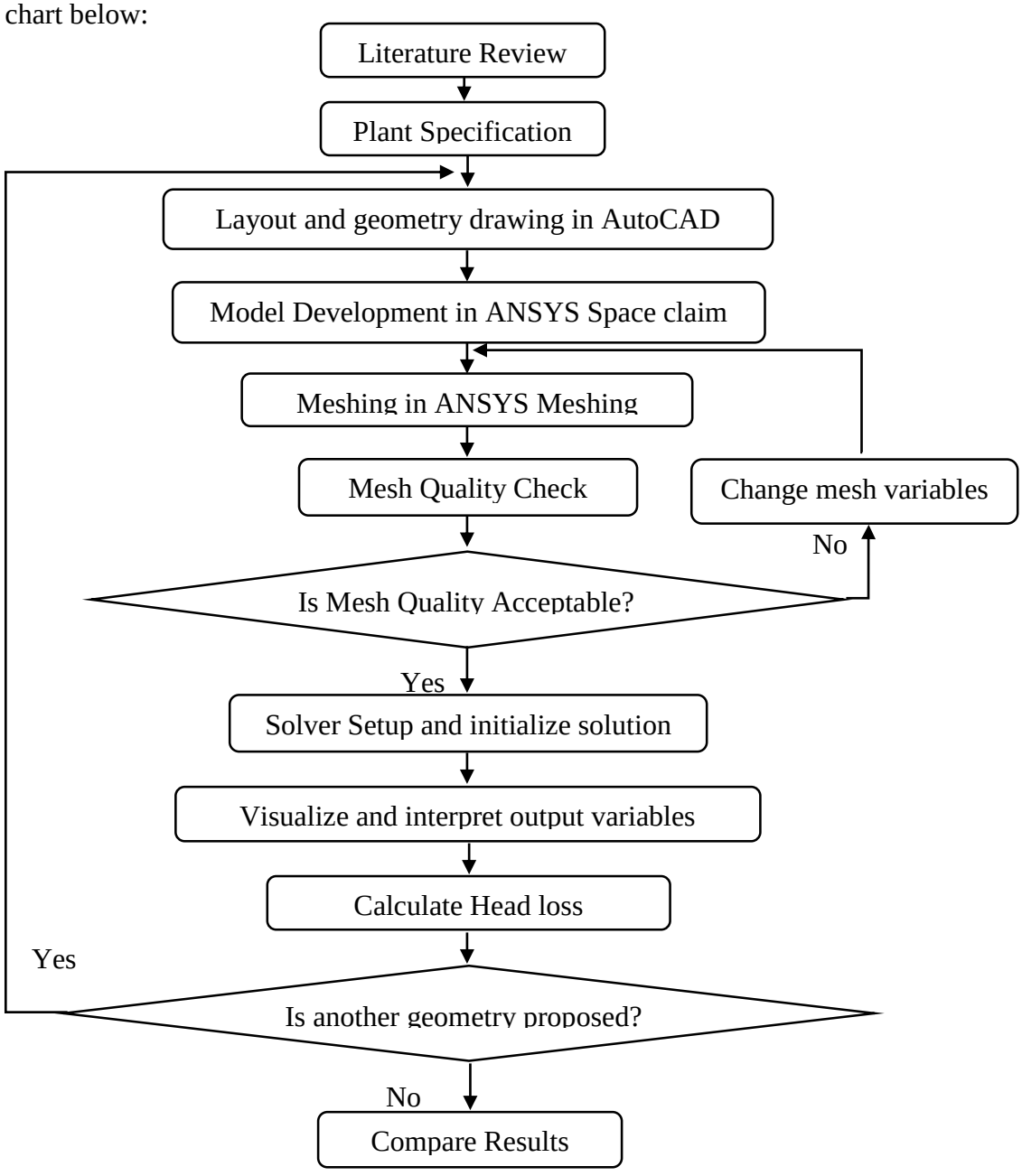

Figure 3. 1: Methodology Flowchart

3.2 Literature Review

A considerable portion of the research was covered by the literature review. Books, journals, papers and articles were thoroughly studied and reviewed. The literature mainly focusing on the penstock pipe, bifurcation, head losses in the pipes and bifurcation, flow distribution due to different geometry of bifurcation and different layout of the manifold, turbulence models, factors contributing head loss and possible measures of head loss reduction were thoroughly studied to obtain the required background for the research. Moreover, Codes, Design guidelines were also referred to for industrial design practices. Working principle of CFD Code and ANSYS Fluent software has also been studied.

3.3 Plant Specifications

The specifications of the hydropower plant considered as the case were obtained. The parameters that were considered has been presented in the table 3.1.

Table 3.1: Specifications of model bifurcation

S. No.	Item	Specification
1	Name of Project	Daram Khola Hydropower Project
2	Installed Capacity	9.6MW
4	No. of Generating Units	2
5	Design Discharge per unit	5.15m^3/sec
6	Rated static Net Head	111.2m
7	Inlet Pipe Diameter	1800mm
8	Outlet Pipe Diameter	1275mm
11	Angle of Bifurcation	60°

3.4 Layout and Geometry Drawing

Since the layout is restricted by the site condition, orientation of inlet pipe and placement of turbine inlets, different layouts were proposed matching to the restrictions and the bifurcation geometry conforming to the layout was prepared in AutoCAD software. The bifurcation geometry used in the different symmetric layouts is the same (with bifurcation angle of 60°) and the bifurcation geometry used in asymmetric layouts are different with angle varying according to layout selection. The constraints of site is shown in figure 3.2.

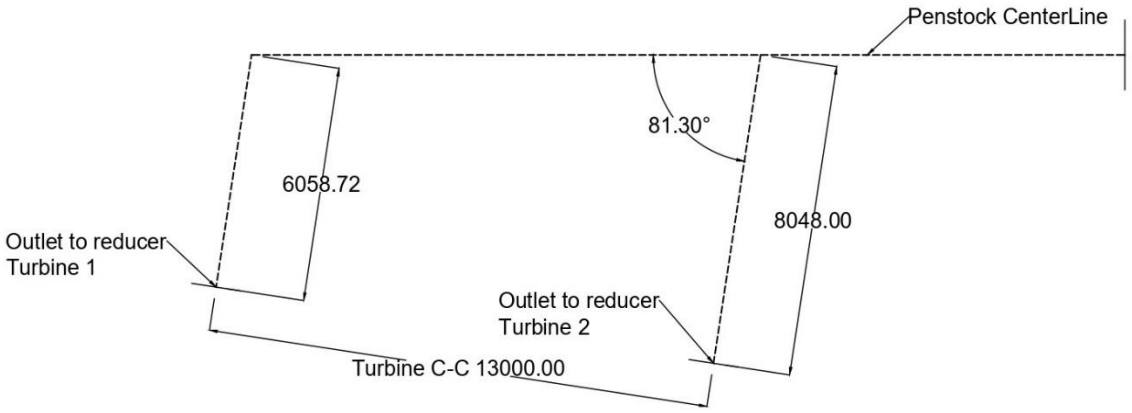

Figure 3. 2: Constraints for bifurcation layout

3.5 Model Development in ANSYS Space claim

The solid model of the whole layout along with the bifurcation was developed in the built-in modeling tool of ANSYS i.e. SpaceClaim. Dimensions were referred from the AutoCAD drawings for convenience.

3.6 Meshing in ANSYS Meshing

The developed model was opened in the Meshing platform of ANSYS Fluent and mesh was generated on the model. The meshing operation divides the control volume of fluid domain into small elements of finite size interconnected in the nodes. Tetrahedral element was used for simplicity in meshing it leads some degree of mass imbalance. The mass imbalance can be controlled by further fine meshing.(Malik & Paudel, 1970). Mesh independence test was carried out to ensure that the results obtained from the simulation does not depend on the mesh size. Inflation Layers are generated in the cylindrical sections near the walls so that the actual fluid behavior at the wall are properly calculated and errors are minimized. The first layer thickness of the inflation layer was given to be 2mm and a total of 10 layers with a growth rate of 1.2 were adopted.

3.7 Mesh Quality Check

The quality of the mesh generated was checked using the mesh metrics. Skewness and orthogonality are the major quality metrics that were monitored. The maximum value of skewness was taken below 0.90 and the mesh exceeding that value was refined by further

processing and change in mesh sizing, inflation layers, etc. The value of orthogonality was monitored so that mesh with low orthogonality can be revised.

3.8 Setup

The Setup is carried out in ANSYS Fluent where the generated mesh is provided with boundary conditions and other necessary input. Water has been chosen as the fluid body. Steady state pressure based solver is incorporated in the Fluent platform. . Other relevant parameters used in the setup and simulation process are as follows:

3.8.1 Turbulence Model

The choice of turbulence model is also important. The models mainly used in industrial CFD are two-equation turbulence models such as k-omega and k-epsilon models or the combination of them like the SST model (Casartelli & Ledergerber, 2006). K-epsilon turbulence model has been used to model the flow of turbulence in the fluid domain. Standard wall function is incorporated with the K-epsilon turbulence model

3.8.2 Wall Roughness

The wall roughness coefficient of 0.1mm is selected for the frictional head loss. Rest of the calculation such as relative roughness coefficient, Reynolds' number and friction factor will be done by the software itself.

3.8.3 Reference Pressure

The reference pressure is considered to be 1 atmospheric pressure.

3.8.4 Boundary Conditions

The most important part in conduction a CFD analysis is defining the boundary conditions. The boundary conditions provided determines the nature of the fluid and the solution of the problem. It is giving the fluid flow governing equations with distinct values of some variables such as pressure, mass flow rate, velocity or some other parameters at the boundaries. In this case, the conditions known at the boundaries can be the pressure, velocity profile or the total flow rate. The conditions at the outlets are unknown and the solver is responsible for calculating the values of fluid variables at the inlet, outlet and overall fluid domain. Mass flow rate at inlet and the pressure at outlet were provided as the

boundary conditions. No slip condition was used for walls, with a wall roughness height of 0.1mm.

3.8.5 Residuals

The residual is the measure of the local imbalance of a conserved variable in each control volume. The value of residual to be achieved depends on the accuracy of result desired. The smaller the value of residual, the more accurate the solution is. However, it takes more time and computational power to achieve smaller values of residual. In this case, a residual value of 0.00001 was considered, which can be further decreased to improve the accuracy of results.

3.9 Simulation

Flow simulation was done using the Computational fluid Dynamics approach in ANSYS Fluent. In this process, the governing equations of fluid flow are solved in a numerical method approach taking the values provided as the boundary conditions. In this case, the mass flow rate at inlet was given as the inlet boundary condition and the pressure at both outlets was given as 1 atmospheric pressure. Enough number of iterations was run for the solution to converge. In case where the solution did not converge in the given number of iterations, the number of iterations was increased and the calculation was again run until convergence was achieved.

3.10 Flow Analysis

The variables such as Pressure, velocity, turbulence, mass flow rate etc. were monitored to analyze the flow of fluid. Mass flow rate was calculated at the two outlets and compared and the sum was compared with the value at inlet to determine flux imbalance. Area weighted average pressure and area weighted average velocity at inlet and outlets were calculated (result provided by ANSYS) to determine the head loss in the bifurcation layout. Different contours of variables like pressure, velocity, turbulence etc. with color mappings were analyzed to determine the flow behavior and consider the need for revision in the layout and geometry of the bifurcation.

3.11 Head Loss Calculation

Head loss value for each outlet was calculated by the difference between the total head at the inlet and the total head at the outlet.

Total head of a fluid in motion is the sum of its potential head, velocity head and pressure head. Mathematically

$$\text{Total head, } H = z + \frac{V^2}{2g} + \frac{p}{\rho g} \text{ m} \qquad \text{Equation 3.1}$$

Hence, the total head at inlet, outlet 1 and outlet 2 are given by equation 3.2, 3.3 and 3.4 respectively.

$$H_i = z_i + \frac{V_i^2}{2g} + \frac{p_i}{\rho g} \qquad \text{Equation 3.2}$$

$$H_1 = z_1 + \frac{V_1^2}{2g} + \frac{p_1}{\rho g} \qquad \text{Equation 3.3}$$

$$H_2 = z_2 + \frac{V_2^2}{2g} + \frac{p_2}{\rho g} \qquad \text{Equation 3.4}$$

The head loss for outlet 1 and outlet 2 can be calculated as:

$$\Delta H_1 = H_i - H_1$$

$$= \left(z_i + \frac{V_i^2}{2g} + \frac{p_i}{\rho g}\right) - \left(z_1 + \frac{V_1^2}{2g} + \frac{p_1}{\rho g}\right)$$

Since the bifurcation manifold is in horizontal arrangement and there is no change in height between inlet and outlets, the potential head are same for inlet and outlet. Therefore,

$$\Delta H_1 = \left(\frac{V_i^2}{2g} + \frac{p_i}{\rho g}\right) - \left(\frac{V_1^2}{2g} + \frac{p_1}{\rho g}\right) \qquad \text{Equation 3.5}$$

$$\Delta H_2 = \left(\frac{V_i^2}{2g} + \frac{p_i}{\rho g}\right) - \left(\frac{V_2^2}{2g} + \frac{p_2}{\rho g}\right) \qquad \text{Equation 3.6}$$

3.12 Conduct the whole Process for another layout

The whole process explained in the methodology section was repeated for all the layouts proposed and the head loss and flow distribution pattern of each layout was evaluated.

3.13 Comparison of results

The value of head loss in each layout was compared to determine the flow having minimum head loss. Similarly, the non-uniform distribution of flow causes the difference between the mass flow rates of the two outlets. This difference occurring in each layout was compared to determine the layout with best possible distribution of flow.

CHAPTER FOUR: FLOW ANALYSIS

4.1 Mesh Independence Test

Mesh independence test was carried out to ensure that the result obtained from the simulation does not depend on the mesh size. It was performed in the symmetric layout with a bend angle of 24°. The mesh size was decreased from 400mm to 50mm in steps as shown in table 4.1. The mesh size of 60mm was chosen to be used further in this study since the outputs which are inlet pressure and mass flow rate at outlet one are stable in that range. The values of inlet pressure and mass flow rate at outlet 1 for different mesh sizes are presented in table 4.1 and the graphical representations are in figure 4.1 and figure 4.2.

Table 4. 1 Mesh Independence Test Results

Mesh Size (mm)	Inlet Pressure (Pa)	Mass Flow rate at outlet 1 (kg/s)
400	107569.87	4896.1831
300	105650.05	4949.6271
200	104017.13	5045.2255
100	103387.90	5061.6505
90	103368.53	5062.5522
80	103377.05	5064.7138
70	103367.05	5063.2377
60	103358.65	5060.8665
50	103366.90	5061.4394

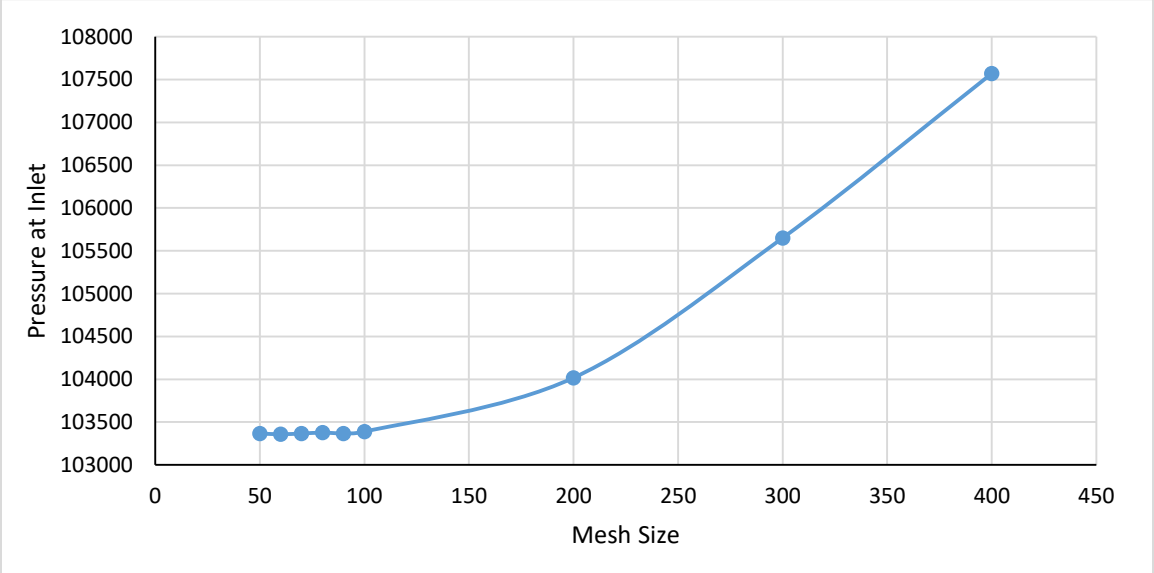

Figure 4. 1: Variation of Inlet pressure with mesh size

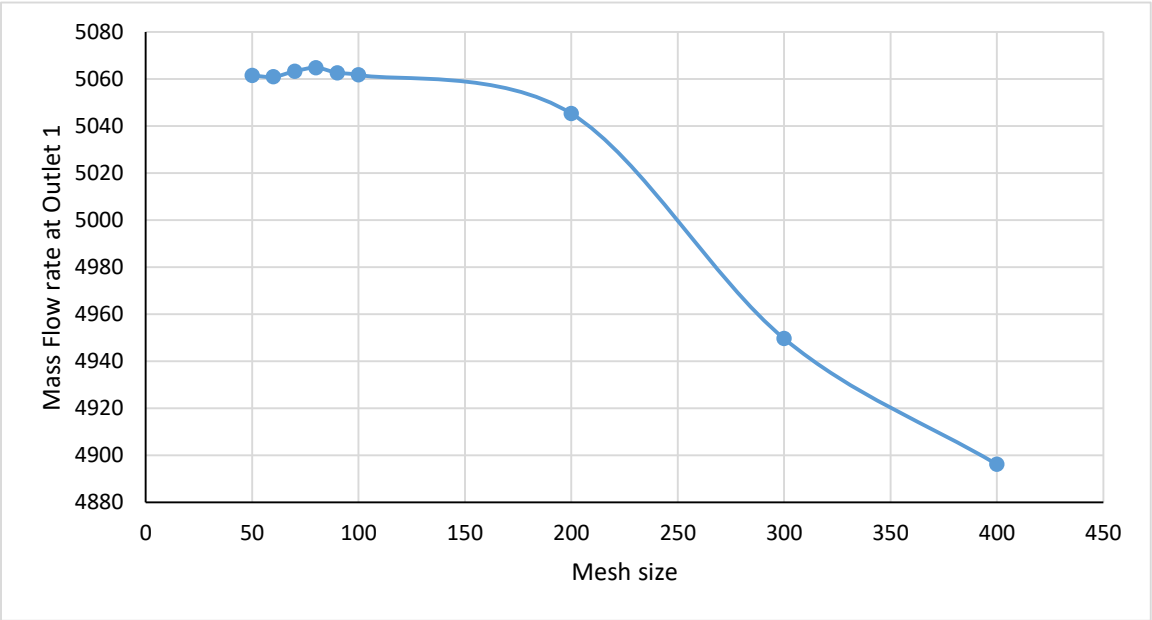

Figure 4. 2: Variation of Mass Flow Rate at outlet 1 with mesh size

4.2 Flow Analysis in Asymmetric Layouts

4.2.1 Asymmetric Layout 1

An initial layout was developed which was totally guided by the geometrical constraints as explained in Figure 3.2. The layout is considered as Layout 1 and presented in Figure 4.3.

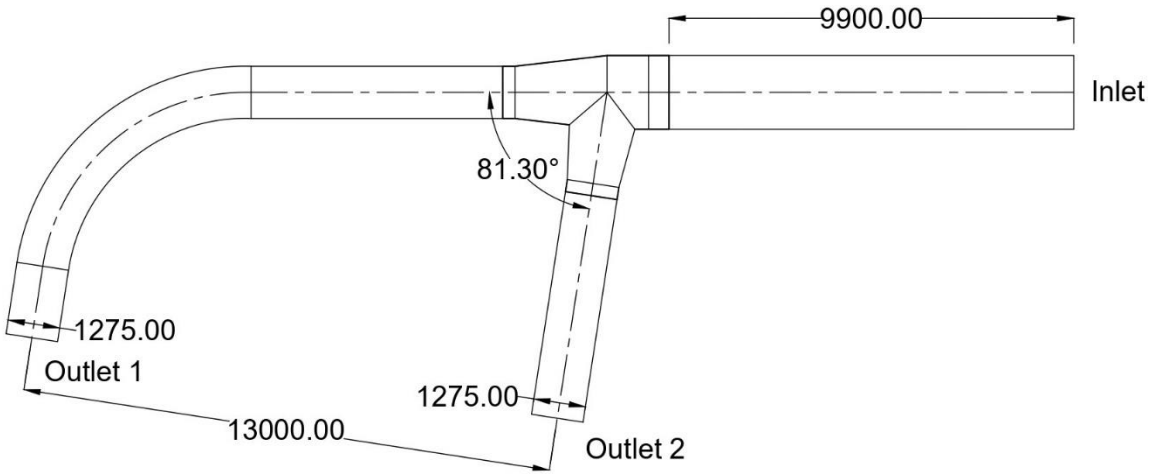

Figure 4.3: Asymmetric Bifurcation Layout (Layout 1)

A 3D model of this layout was developed in ANSYS SpaceClaim which is shown in figure 4.4.

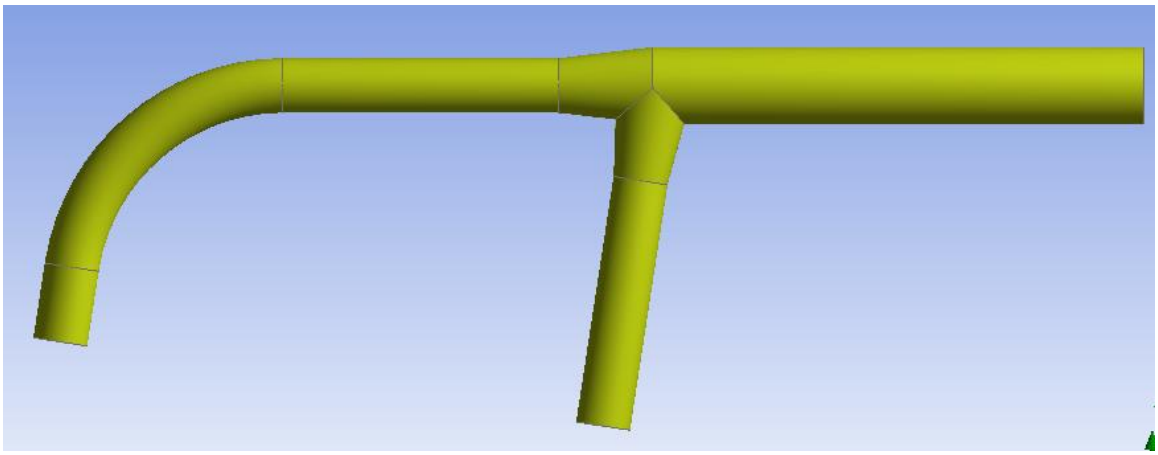

Figure 4. 3: 3D model of layout 1

This model was exported to ANSYS Meshing and a tetrahedral mesh was generated. The quality of mesh was monitored by skewness and orthogonal quality. The Skewness average was found to be 0.18 and the orthogonality average is 0.82 which are acceptable. Inflation Layers are provided with first layer thickness as 1mm, growth rate 1.2 and number of layers equal to 10 in the cylindrical portions to better model the fluid flow near the walls.

The model consists of one inlet and two outlet. Simulation has been performed by using mass flow inlet and constant pressure outlet boundary conditions.

Inlet Boundary Conditions:

Type: Mass Flow Inlet

Value: 10320 kg/s

Normal to Boundary

Turbulence: Viscosity and Hydraulic Diameter

Viscosity: 5%

Hydraulic Diameter: 1.8m

Outlet Boundary Conditions:

Type: Pressure Outlet

Value: 0 Gauge pressure (1 Atm)

Turbulence: Viscosity and Hydraulic Diameter

Viscosity: 5%

Hydraulic Diameter: 1.275 m

Contour Plots

The contour plots of velocity distribution, pressure distribution and the turbulent kinetic energy at mid plane of symmetry were visualized.

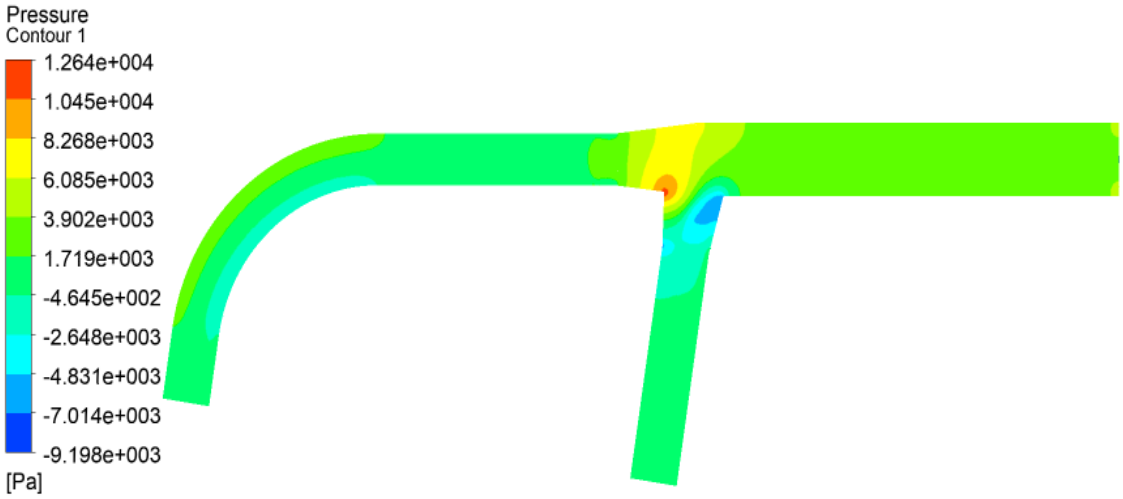

Figure 4. 4: Pressure distribution at plane of symmetry

In pressure distribution diagram, it is observed that the pressure distribution is smooth in the inlet pipe region. In the region of bifurcation, pressure distribution is varied and there exists some high pressure and low pressure regions. The pressure has increased in the crotch region of bifurcation due to effect of stagnation. A low pressure region is developed at the area where the branch pipe at an angle with the inlet pipe is connected. This is due to the sudden expansion effect of the cross section provided by the geometry.

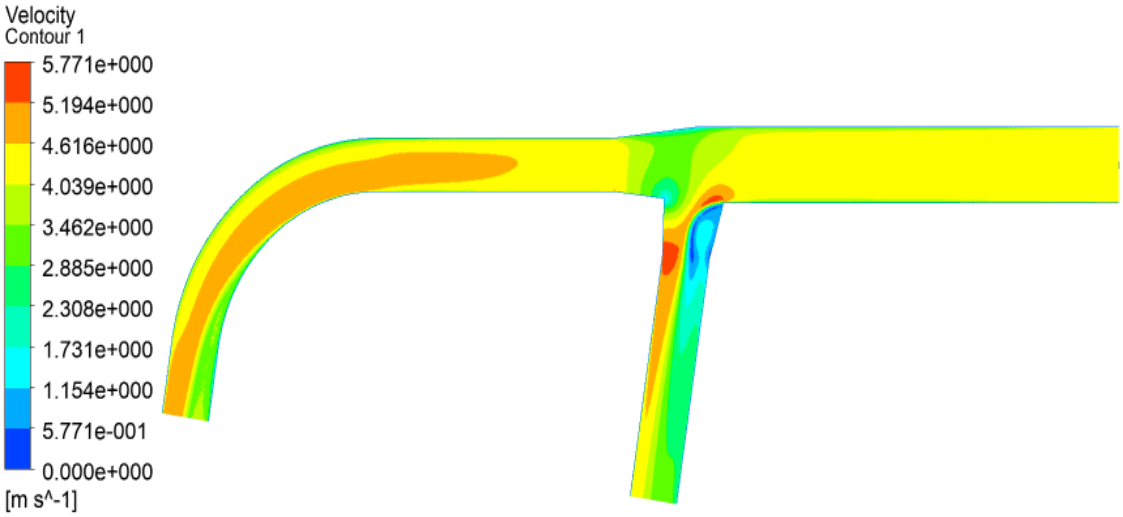

Figure 4. 5: Velocity distribution at plane of symmetry

Similar phenomenon can be observed in the velocity distribution diagram. It is reciprocal of the pressure distribution, i.e. the velocity has increased in the low pressure regions and decreased in the high pressure regions following the Bernoulli's principle. Effect of walls can be observed as there exists low velocity up to a small distance from the wall.

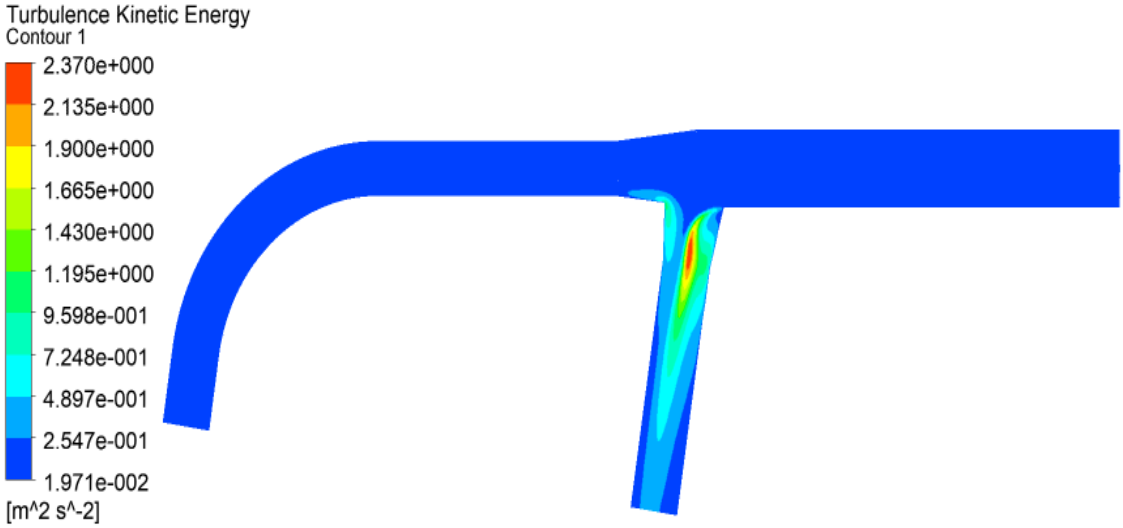

Figure 4. 6: Turbulence distribution at plane of symmetry

In the turbulence kinetic energy (k) visualization, the flow seems laminar in the inlet pipe region and in the straight branch. While in the angled branch, the turbulence has increased to a high value. This also signifies the need for the revision of the geometry by which the turbulence can be decreased.

4.2.2 Asymmetric Layout 2

A revised asymmetric layout was developed, by decreasing the angle of bifurcation to 45° and shifting the position of bifurcation upstream by a distance of 3185mm to conform to the site constraints. This layout is considered as layout 2 and the 2D drawing with relevant dimensions is shown in figure 4.7.

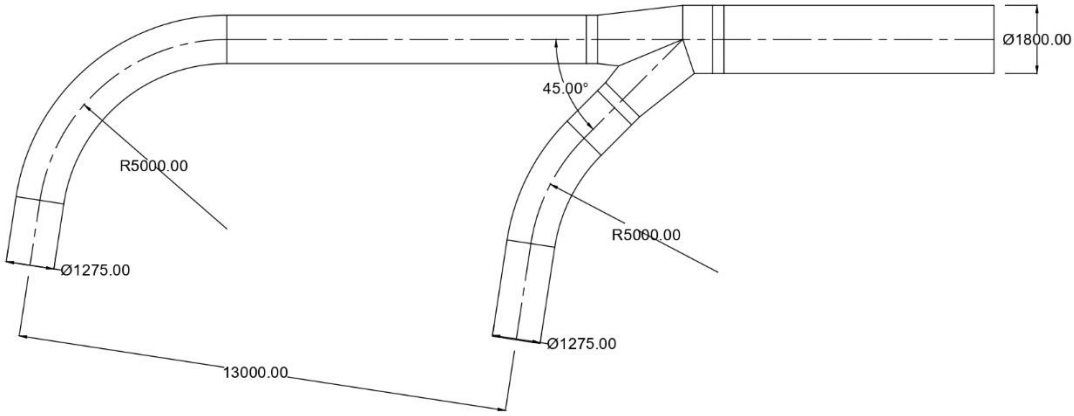

Figure 4. 7: Asymmetric Layout 2

A 3D model was generated in ANSYS SpaceClaim which is shown in figure 4.8.

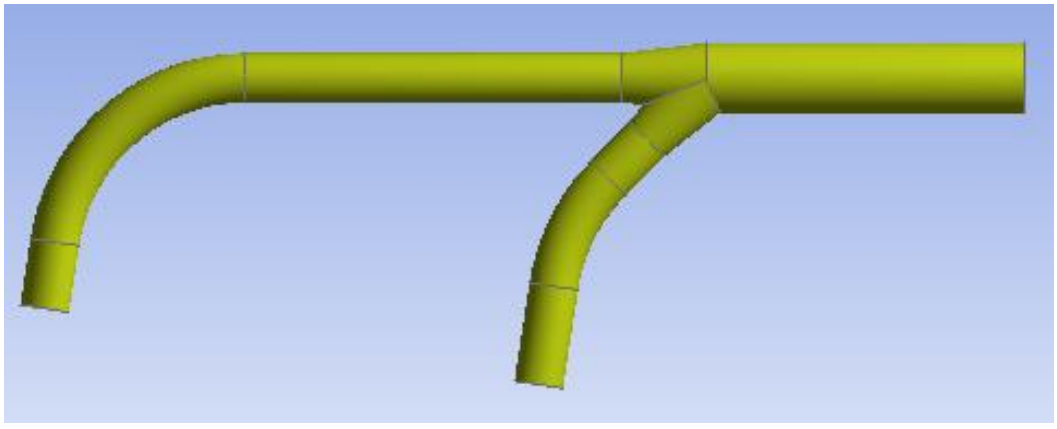

Figure 4. 8: 3D Model of Layout 2

This model was exported to ANSYS Meshing and a tetrahedral mesh was generated. The quality of mesh was monitored by skewness and orthogonal quality. The Skewness average was found to be 0.16 and the orthogonal quality average is 0.84 which are acceptable. Inflation Layers are provided similar to Layout 1.

The model consists of one inlet and two outlet. Simulation has been performed by using mass flow inlet and constant pressure outlet boundary conditions, the values of which are similar to layout 1.

Contour Plots

The contour plots of velocity distribution, pressure distribution and the turbulent kinetic energy at mid plane of symmetry were visualized.

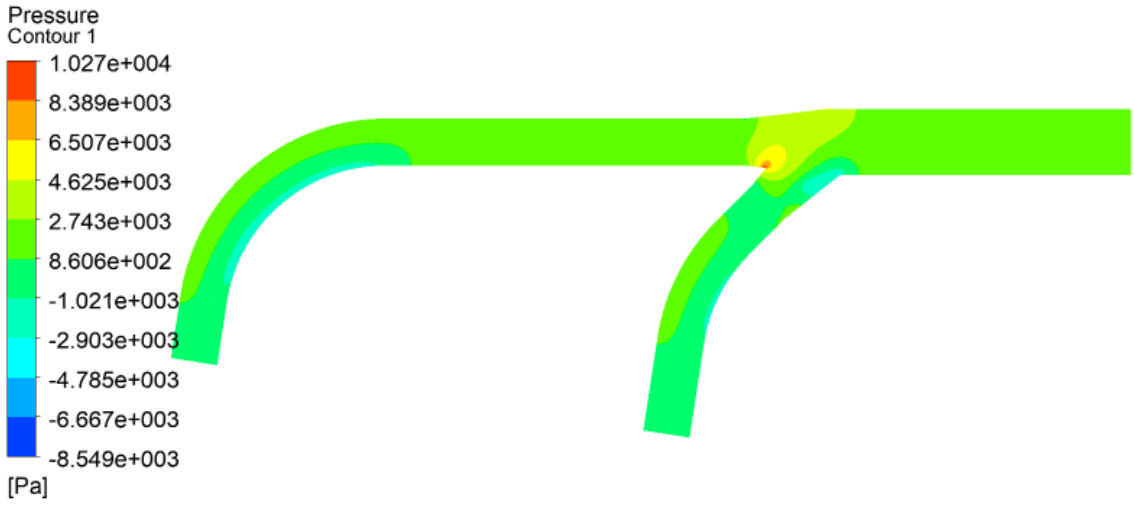

Figure 4. 9: Pressure Distribution at mid-plane

High pressure region at the crotch of the bifurcation was still observed. The low pressure region at the intersection of the angled branch pipe and the main inlet pipe was reduced compared to the same region of layout 1. Another low pressure region was observed at the inner side of bend in the straight branched. The high pressure at the crotch is due to the geometric arrangement where the fluid strikes directly and it cannot be reduced by ordinary means. Other areas contributing to head loss may be reduced by successive revision of the layout geometry.

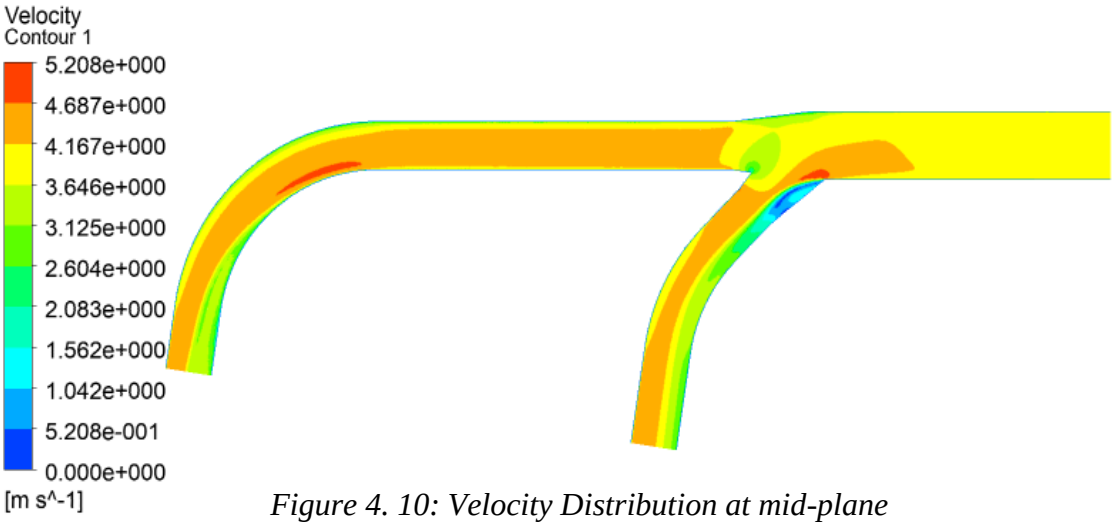

Figure 4. 10: Velocity Distribution at mid-plane

The pressure and velocity distribution shows reciprocal relation. High velocity is observed in low pressure region and low velocity is observed in high pressure region except for the intersection point of angled branch pipe and the main inlet pipe. In that region, both velocity and pressure are observed to attain low value. This is a major cause leading to head loss in that particular region.

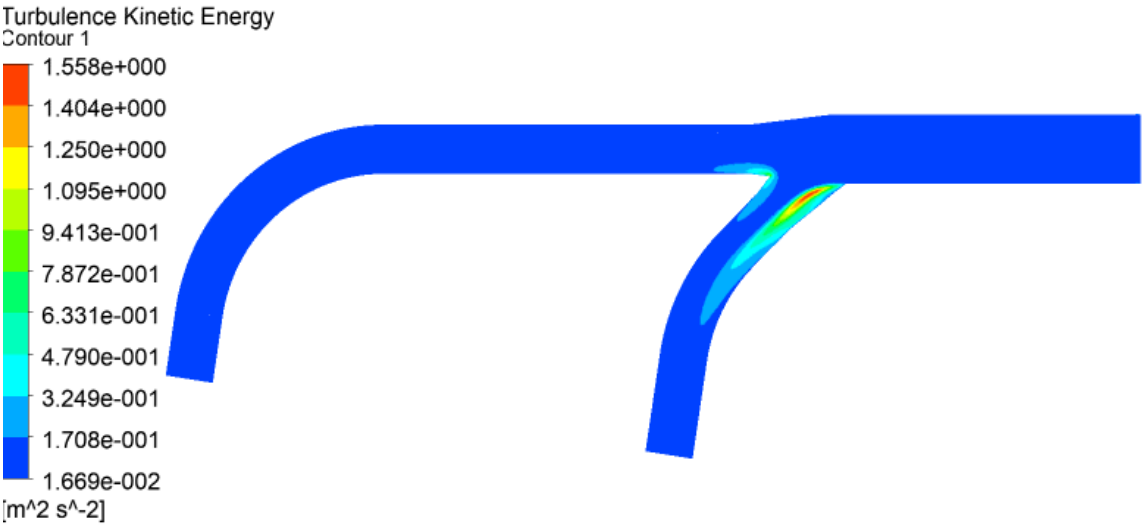

Figure 4. 11: Turbulent kinetic energy (k) Distribution at mid-plane

In the turbulence kinetic energy (k) visualization, the flow seems laminar in the inlet pipe region and in the straight branch. While in the angled branch, the turbulence has increased to a high value. However, it is lower than the turbulence observed in Layout 1.

4.3 Flow Analysis in Symmetric Layout

To compare the flow pattern with varied layouts, a symmetric bifurcation layout was developed, with angle of bifurcation 60°, which was made possible by adding a bend in penstock pipe just upstream of the bifurcation and subsequent changes in the pipe bends downstream in the branch pipes. The angle of upstream bend was measured to be 28.23° on the 2D drawing, which was rounded off to 28° for simplicity. More layouts were developed by changing the bend angle by 1° in each revision, keeping other geographical constraints and the angle of bifurcation constant. The 2D drawing of symmetric layout with upstream bend angle 28° is shown in figure 4.12

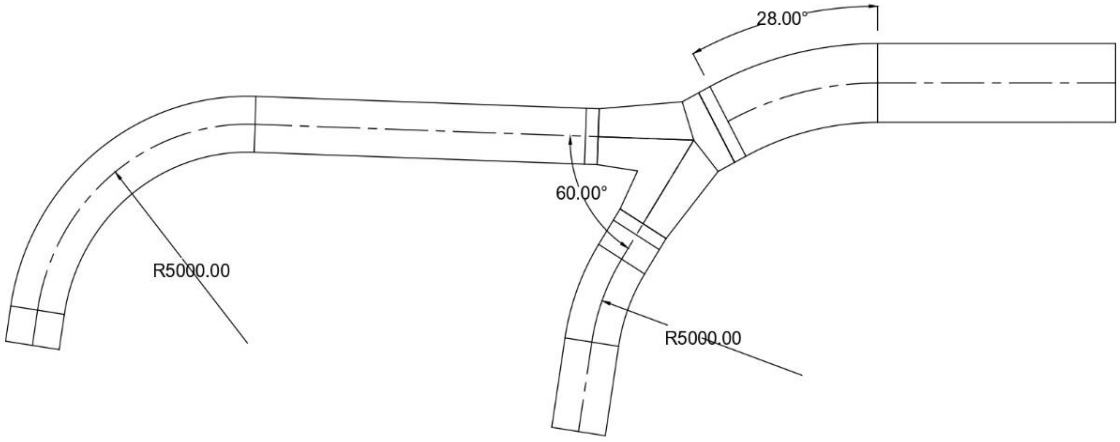

Figure 4. 12: Symmetric Bifurcation Layout

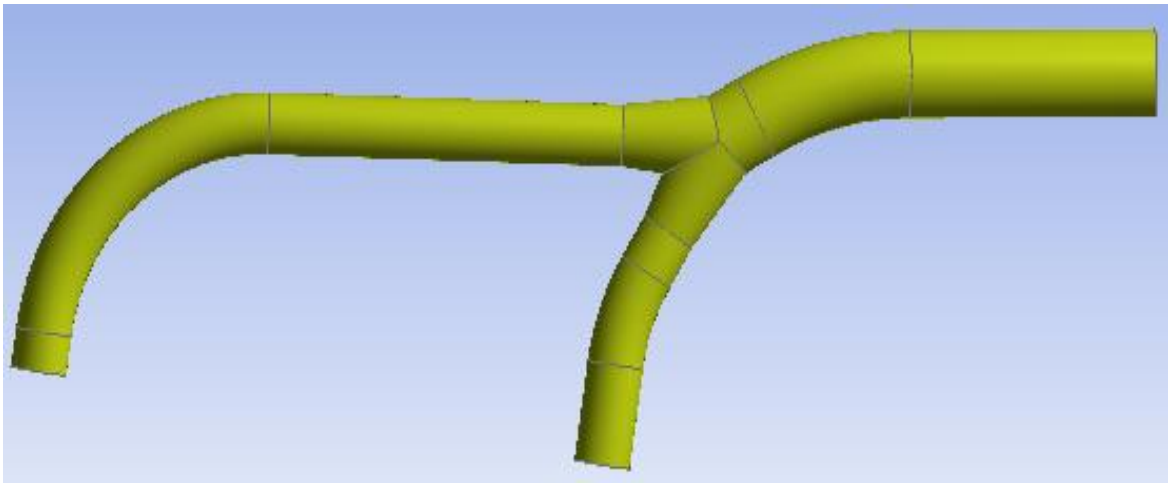

Figure 4. 13: 3D Model of Symmetric Bifurcation Layout

Similar procedure of meshing and simulation was performed with boundary condition similar to the asymmetric layouts. The contour plots obtained are presented in figures below.

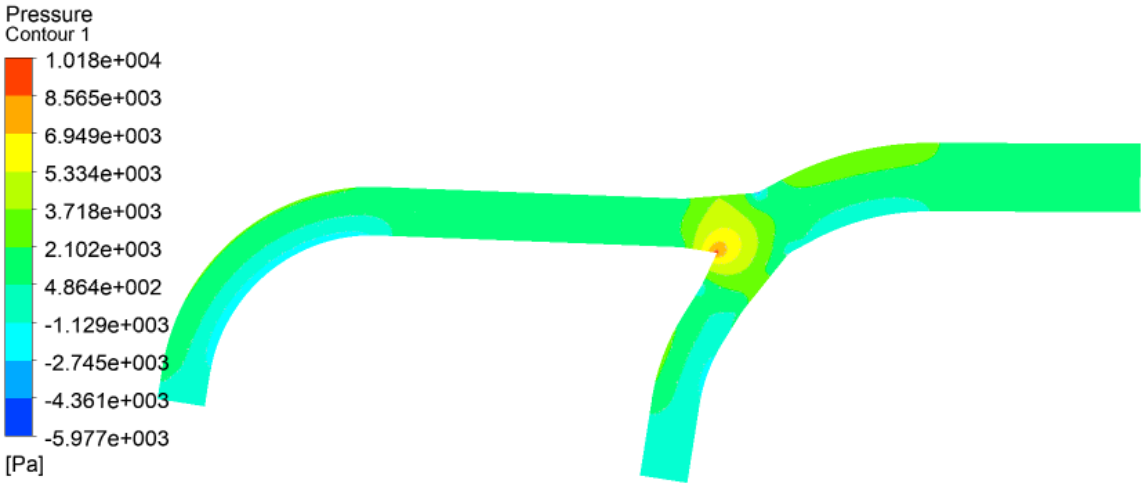

Figure 4. 14: Pressure Distribution at mid plane of symmetric layout

The pressure is distributed more or less uniformly in the two branch pipes, and a single low pressure region as observed in the asymmetrical layouts is not observed in symmetric layout. High pressure at the crotch region is similar for asymmetric and symmetric bifurcations.

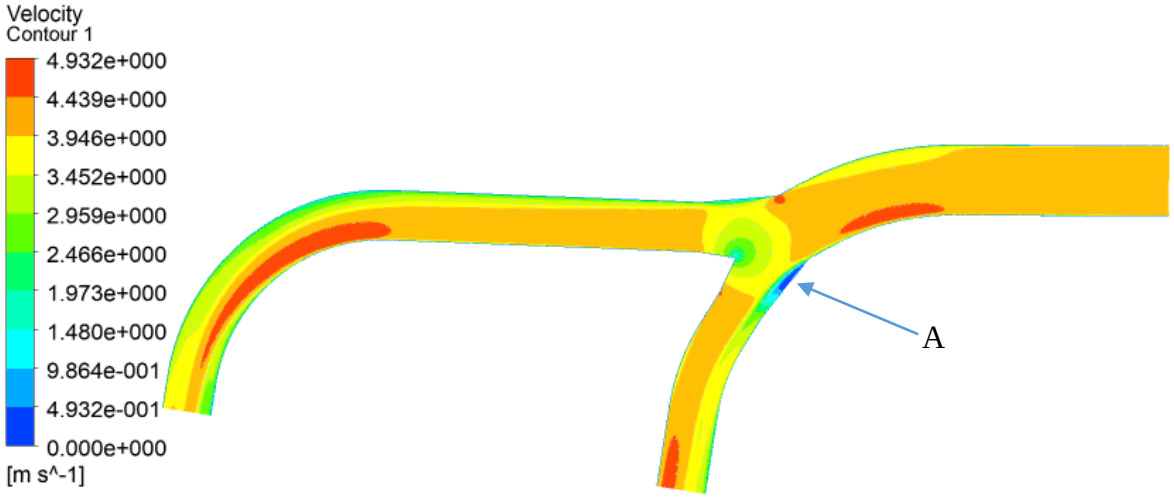

Figure 4. 15: Velocity Distribution at mid plane of symmetric layout

A notable low velocity region is observed at region ‘A’ as shown in figure 4.15. This may be due to higher value of angle of bifurcation which deviates the flow sharply.

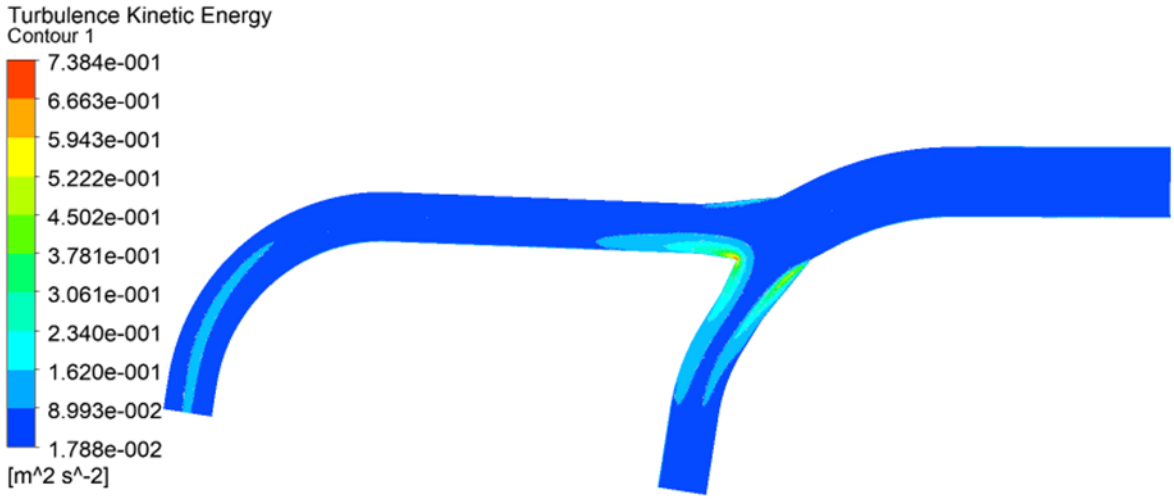

Figure 4. 16: Turbulent kinetic energy distribution at mid plane

The Turbulent kinetic energy is high at the crotch which is the main area of head loss in this case. It is distributed equally into the two branches. Another high turbulence is seen in the branch pipe towards outlet 2.

4.4 Revisions in the Symmetric Layout

The symmetric layout with bend angle 28° was successively revised by changing the bend angle by 1° in each revision. The bend angle was increased up to 32° at highest. Other geometrical correction in the bend angle of branch pipes were done according to requirement. At bend angle of 32°, the radius of bend in the branch pipe towards outlet 2 had to be decreased from 5000mm to 4700 mm to meet other geographical requirements. Hence, the bend angle was not further increased. While revising the layout by decreasing the inlet bend angle, the head loss at outlet 2 kept on increasing rapidly and the direction towards outlet 2 kept on moving away from the turbine inlet location. So, the inlet bend angle was decreased up to 24° and halted. The angle of bifurcation was kept constant at 60°. Simulation was performed in each case and the results were visualized as well as the head loss was calculate for each case. The pressure and velocity contours were similar to

that of the 28° bend layout and were not distinct visually on normal observation. The 2D drawing of the extremities cases (24° and 32°) are shown in figure 4.17 and figure 4.18.

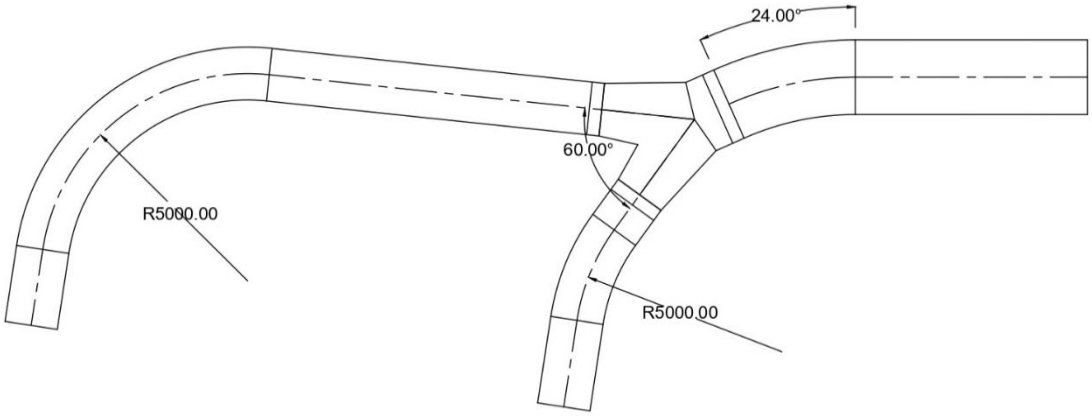

Figure 4. 17: Symmetric bifurcation layout with decreased bend angle

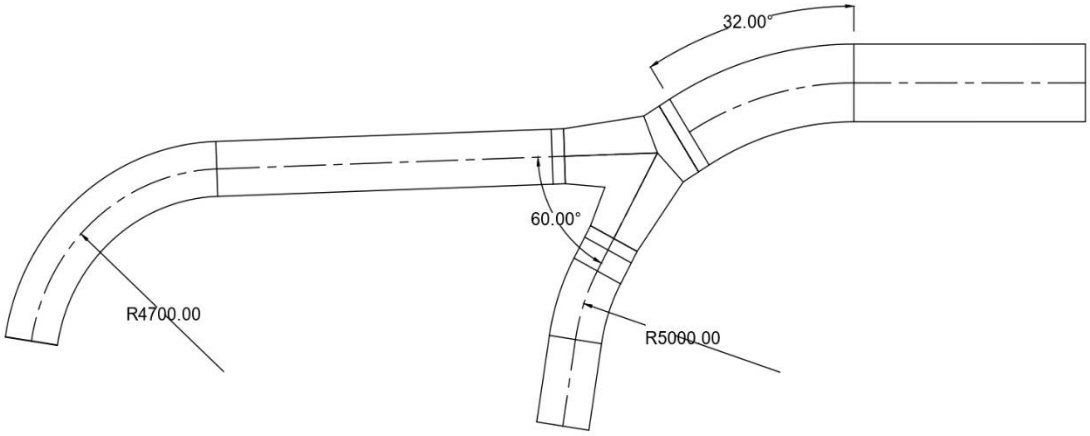

Figure 4. 18: Symmetric bifurcation layout with increased bend angle

CHAPTER FIVE: RESULTS AND DISCUSSION

5.1 Results

5.1.1 Asymmetric Layout 1

After the solution converged to a residual value of 0.00001, different parameters were evaluated at the inlet and the two outlets which are discussed as follows:

Mass Flow Rate:

The mass flow rate of the fluid at the inlet and outlet obtained after simulation are:

Inlet : 10320.0000 kg/s

Outlet 1 : 5574.91 kg/s

Outlet 2 : 4745.08 kg/s

Mass Imbalance: 0.0002 kg/s

Area Weighted Average Pressure

Inlet : 105248.51 pa

Outlet 1 : 101325 pa

Outlet 2 : 101325 pa

Area Weighted Average Velocity

Inlet : 4.065844 m/s

Outlet 1 : 4.4016987 m/s

Outlet 2 : 3.7302175 m/s

Head Loss Calculation

Head loss in the system was calculated by the difference between the total head (sum of pressure head and velocity head) at inlet and the sum of the total head at the two outlets.

Table 5 1: Head loss calculation for Asymmetric Layout 1

S.N.	Particular	Unit	Inlet Pipe	Outlet - 1	Outlet-2
1.a	Area Weighted Average Pressure from CFD Analysis	Pa	105,248.00	101,325.00	101,325.00
b	Area Weighted Average Velocity from CFD Analysis	m/s	4.07	4.40	3.73
c	Pipe Diameter		1.80	1.275	1.275
d	Calculated Flow Rate	m3/sec	10.35	5.62	4.76
e	Calculated Static Head	m	10.75	10.35	10.35
f	Velocity Head	m	0.84	0.99	0.71
g	Total Head	m	11.59	11.33	11.06
2	Head Loss	m		0.26	0.5340
3.a	Design Discharge	m3/s	10.30	5.15	5.15
b	**Head Loss @ Design Discharge**	**mm**		**214.70**	**624.38**

5.1.2 Asymmetric Layout 2

After the solution converged to a residual value of 0.00001, different parameters are evaluated at the inlet and the two outlets which are discussed as follows:

Mass Flow Rate:

The mass flow rate of the fluid at the inlet and outlet obtained after simulation are:

Inlet : 10320.0000 kg/s

Outlet 1 : 5184.7437 kg/s

Outlet 2 : 5135.2564 kg/s

Mass Imbalance: 0.0001 kg/s

Area Weighted Average Pressure

Inlet : 103804.83 pa

Outlet 1 : 101325 pa

Outlet 2 : 101325 pa

Area Weighted Average Velocity

Inlet : 4.0658441 m/s

Outlet 1 : 4.0946725 m/s

Outlet 2 : 4.0353421 m/s

Head Loss Calculation

Head loss in the system is calculated by the difference between the total head (sum of pressure head and velocity head) at inlet and the sum of the total head at the two outlets.

Table 5 2: Head loss calculation for Asymmetric Layout 2

S.N.	Particular	Unit	Inlet Pipe	Outlet - 1	Outlet-2
1.a	Area Weighted Average Pressure from CFD Analysis	Pa	103,804.83	101,325.00	101,325.00
b	Area Weighted Average Velocity from CFD Analysis	m/s	4.06	4.09	4.04
c	Pipe Diameter		1.80	1.275	1.275
d	Calculated Flow Rate	m3/sec	10.34	5.23	5.15
e	Calculated Static Head	m	10.60	10.35	10.35
f	Velocity Head	m	0.84	0.85	0.83
g	Total Head	m	11.44	11.20	11.18
2	Head Loss	m		0.24	0.27
3.a	Design Discharge	m3/s	10.30	5.15	5.15
b	**Head Loss @ Design Discharge**	**mm**		**233.61**	**265.09**

Mathematical Calculation

The head loss coefficient for outlet 2 of asymmetric layout 2 was calculated using the values obtained from simulation results.

From equation 2.6, we have

$$\Delta H = \alpha \frac{V_0^2}{2g}$$

Where α is the head loss coefficient.

The head loss coefficient is given by,

$$\alpha = \frac{2g * \Delta H}{V_0^2} \qquad \text{Equation 5.1}$$

$$= \frac{2 * 9.81 * 0.26509}{(4.035^2)} = 0.3194$$

Also, the head loss coefficient for the same outlet was calculated using experimental graphs and mathematical formula for friction head loss. For this purpose, the model is divided into four parts that are: the main inlet pipe upto bifurcation, the bifurcation, the straight pipes in the branch towards outlet 2 and the bend pipe in the branch towards outlet 2.

(i) Main Inlet pipe up to bifurcation

In this section, the head loss is due to friction loss in the pipe which can be calculated by the Darcy-Weisbach formula expressed as in equation 2.8.

$$h_f = \frac{4fLV^2}{2gD}$$

Where 4f is friction factor which is a function of Reynolds' number and the ratio of roughness height and pipe diameter. In this case, the friction factor is obtained from Moody diagram equal to 0.11. Hence, the head loss is,

$$h_f = \frac{0.11 * 7.14 * 4.0476^2}{2 * 9.81 * 1.8} = 0.0364$$

From equation 5.1, the head loss coefficient is calculated to be equal to 0.0436.

(ii) Bifurcation

The head loss in a 45° bifurcation is determined using the experimental chart provided by D.S. Miller as shown in figure 2.4. The ratio of area of the outlet and that of inlet is equal to 0.5. Assuming the flow rate in branch to be half of the inlet pipe flow rate, the head loss coefficient is determined to be 0.11.

(iii) Bend pipe in the branch towards outlet 2

The head loss coefficient of bend is determined with the help of figure 2.5. Fore a bend angle of 36.3° and ratio of bend radius to pipe diameter (r/d) of 3.92, the head loss coefficient of bend is determined to be 0.08.

(iv) Straight pipes in the branch towards outlet 2

Using equation 2.8 and equation 5.1, the head loss coefficient for this portion was calculated to be 0.06857

Hence, the actual head loss coefficient for outlet 2 is given by the sum of the head loss coefficients for each discrete section, which is calculated to be equal to 0.3022.

Comparison

Comparing the head loss coefficient obtained from simulation results and the head loss coefficient calculated by mathematical and experimental literature,

α_s = 0.3194 (obtained from simulation results)

α_m = 0.3022 (obtained from mathematical calculation)

Percentage error = $\frac{\alpha_s - \alpha_m}{\alpha_s} * 100\%$

$= \frac{0.3194 - 0.3022}{0.3194} * 100\%$

$= 5.38\ \%$

The difference between simulation results and mathematical results is 5.38% which is in acceptable range.

5.1.3 Symmetric Layout (Bend Angle 28°)

After the solution converged to a residual value of 0.00001, different parameters were evaluated at the inlet and the two outlets which are discussed as follows:

Mass Flow Rate:

The mass flow rate of the fluid at the inlet and outlet obtained after simulation are:

Inlet : 10320.0000 kg/s

Outlet 1 : 5079.6260 kg/s

Outlet 2 : 5240.3741 kg/s

Mass Imbalance: 0.0001 kg/s

Area Weighted Average Pressure

Inlet : 103332.01 pa

Outlet 1 : 101325 pa

Outlet 2 : 101325 pa

Area Weighted Average Velocity

Inlet : 4.0659101 m/s

Outlet 1 : 4.0002007 m/s

Outlet 2 : 4.1203819 m/s

Head Loss Calculation

Head loss in the system is calculated by the difference between the total head (sum of pressure head and velocity head) at inlet and the sum of the total head at the two outlets.

Table 5 3: Head loss calculation for Symmetric Layout

S.N.	Particular	Unit	Inlet Pipe	Outlet - 1	Outlet-2
1.a	Area Weighted Average Pressure from CFD Analysis	Pa	103,332.01	101,325.00	101,325.00
b	Area Weighted Average Velocity from CFD Analysis	m/s	4.07	4.00	4.12
c	Pipe Diameter		1.80	1.275	1.275
d	Calculated Flow Rate	m3/sec	10.35	5.11	5.26
e	Calculated Static Head	m	10.55	10.35	10.35
f	Velocity Head	m	0.84	0.82	0.87
g	Total Head	m	11.39	11.16	11.21
2	Head Loss	m		0.23	0.18
3.a	Design Discharge	m3/s	10.30	5.15	5.15
b	**Head Loss @ Design Discharge**	**mm**		**235.87**	**174.64**

5.1.4 Revised Symmetric Layouts

The symmetrical layout was revised as mentioned in section 4.4. The mass flow rate, velocity and pressure at the inlet and two outlets are presented in this section.

Mass Flow Rate

The mass flow rate at the two outlets, and their difference, for different values of angle of upstream bend are presented in table 5.4.

Table 5 4: Mass flow rate at two outlets for different bend angle

Angle (°)	Mass Flow Rate (kg/s)			
	Outlet 1 (m_1)	Outlet 2 (m_2)	Difference (m_2-m_1)	Inlet
24	5060.867	5259.134	198.267	10320
25	5069.738	5250.262	180.523	10320

26	5072.401	5247.599	175.198	10320
27	5078.851	5241.149	162.297	10320
28	5079.626	5240.374	160.748	10320
29	5082.402	5237.598	155.195	10320
30	5087.489	5232.511	145.022	10320
31	5089.586	5230.414	140.827	10320
32	5088.526	5231.474	142.947	10320

The mass flow rate at the two outlets was observed to vary with the change in bend angle. The difference in mass flow rate at two outlets (m_2-m_1) was plotted against the bend angle to obtain a graph as shown in figure 5.1.

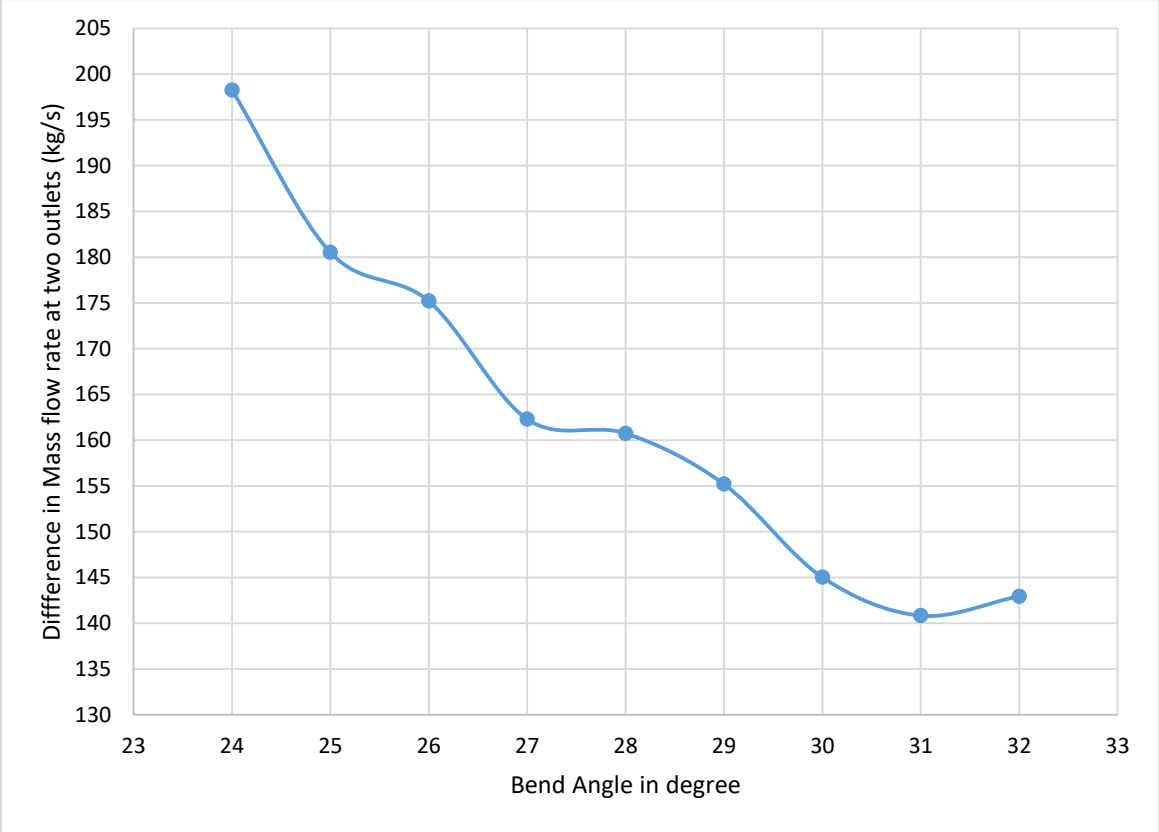

Figure 5. 1: Variation of difference in mass flow rate with bend angle

Velocity

The velocity at the two outlets and at the inlet for different values of bend angle are presented in table 5.5. These values were further used in the calculation of head loss for each case.

Table 5.5: Velocity at inlet and two outlets for different bend angles

	Velocity (m/s)		
Angle (°)	Inlet	Outlet 1	Outlet 2
24	4.06591	3.98292	4.13498
25	4.06591	3.99038	4.12795
26	4.06591	3.99296	4.12592
27	4.06591	3.99880	4.12087
28	4.06591	4.00020	4.12038
29	4.06591	4.00362	4.11835
30	4.06591	4.01033	4.11445
31	4.06591	4.01128	4.11287
32	4.06591	4.02327	4.11384

Pressure

The value of pressure obtained at the two outlets and the inlet after simulation are presented in table 5.6. It can be noted that the value of pressure at both the outlets is equal to 1 atmospheric pressure which was provided as the boundary condition.

Table 5.6: Pressure at inlet and two outlets for different bend angles

	Pressure (Pa)		
Angle	Inlet	Outlet 1	Outlet 2
24	103358.65	101325	101325
25	103358.04	101325	101325
26	103348.19	101325	101325
27	103338.48	101325	101325
28	103332.01	101325	101325
29	103316.40	101325	101325
30	103314.51	101325	101325
31	103316.38	101325	101325
32	103328.35	101325	101325

Head Loss

Value of head loss in mm was calculated for both the outlets by subtracting the total head available at the outlet from the total head available at the inlet in each case. The calculated values are presented in table 5.7.

Table 5.7Head loss for outlet 1 and outlet 2 for different bend angles

Angle (°)	Head Loss (mm)	
	Outlet_1	Outlet_2
24	248.9224	171.0808
25	243.8262	173.4967
26	241.4181	173.5198
27	237.2833	175.0305
28	235.8656	174.6372
29	232.4281	174.0984
30	228.6809	175.8132
31	228.3718	176.7687
32	223.3087	177.4699

The head loss at the two outlets was observed to vary with the change in bend angle. The variation of head loss with bend angle is plotted in separate graphs for outlet 1 and outlet 2 which are presented in figure 5.2 and 5.3 respectively.

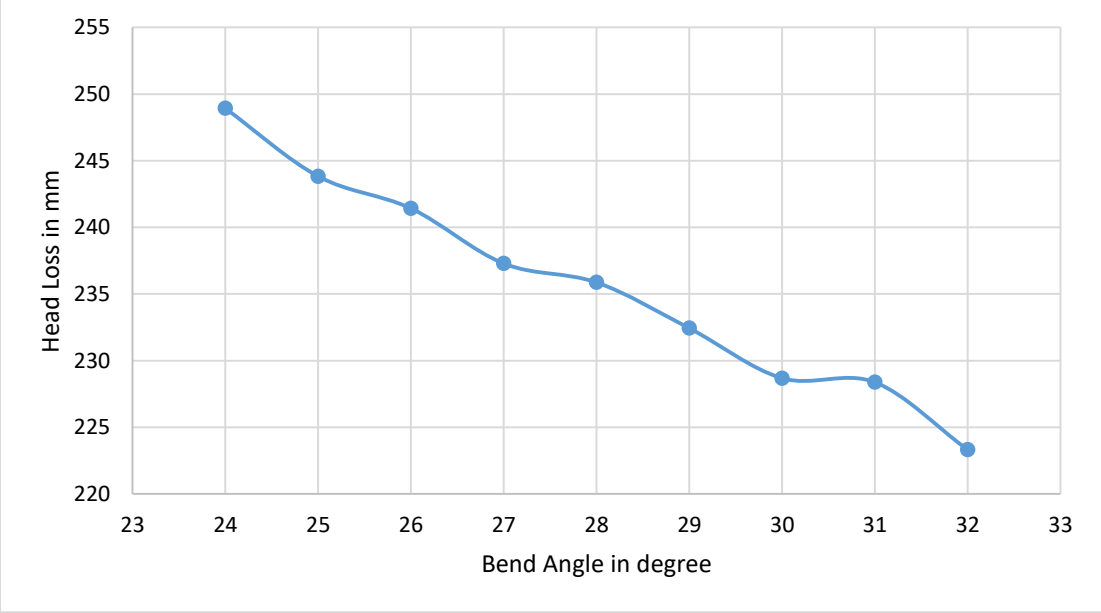

Figure 5. 2: Head loss v/s bend angle for outlet 1

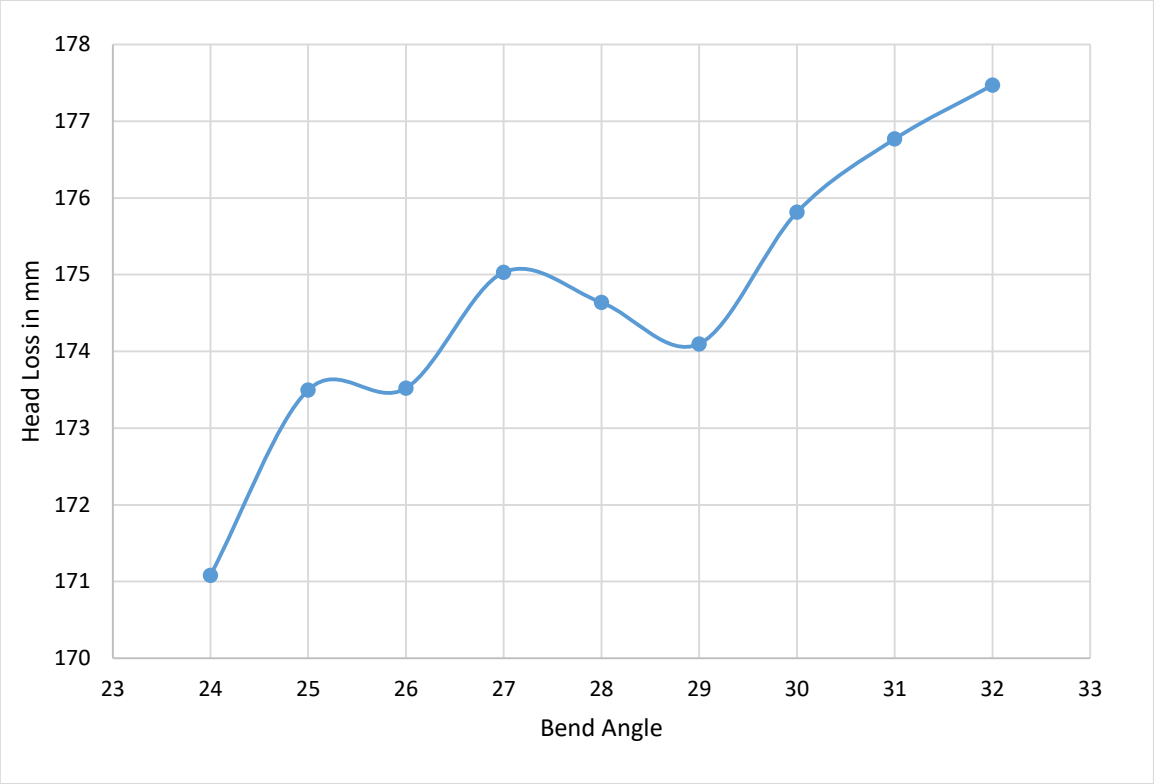

Figure 5. 3: Head loss v/s bend angle for outlet 2

5.2 Discussion

5.2.1 Comparison of Flow Distribution

The flow distribution pattern of the asymmetric layout 1 and asymmetric layout 2, when compared with the reference of velocity contour, reveals that the flow is more uniformly distributed in the layout 2, which has the bifurcation of angle 45°. While in the symmetric layout, where a bend is introduced upstream of the bifurcation, the flow distribution varied with the change in bend angle. The best possible flow distribution in the considered range of varying bend angle from 24° to 32°, was found at a bend angle of 31° where the difference between the flow rate at outlet 1 and flow rate at outlet 2 was 140.83kg/s. The flow distribution of asymmetric layouts 1 and 2 and symmetric layout with bend angle 31° are compared in table 5.8.

Table 5 8: Flow distribution comparison for different layouts

Mass Flow Rate	Asymmetric Layout 1	Asymmetric Layout 2	Symmetric Layout (31° bend)
Inlet (kg/s)	10320	10320	10320
Outlet 1 (kg/s) (m_1)	5574.9120	5184.7437	5089.5862
Outlet 2 (kg/s) (m_2)	4745.0870	5135.2564	5230.4134
Flux Imbalance (kg/s)	0.001	0.0001	0.0004
Mod (m_1-m_2)	829.825	49.4873	140.826

The numerical values of the mass flow rate at outlet 1 and outlet 2 for different layouts reflect that the flow distribution is unequal and there is scope for the revision of the layout and geometry to overcome such unequal flow. Similarly, the numerical values of the mass flow rate at outlet 1 and outlet 2 for Asymmetric Layout 2 is more balanced than the other cases. The flow is still distributed unequally but it has much better behavior than the results of other layouts.

5.2.2 Comparison of Head Loss

The head loss for outlet 1 and outlet 2 in asymmetric layout 1 was observed to differ largely. While in the case of asymmetric layout 2 the head loss in the two outlets attain a value closer to each other. In the case of symmetric layout, while varying the bend angle, the head loss for outlet 1 decreased with an increase in bend angle, while the head loss for outlet 2 increased with an increase in bend angle. An optimum value is obtained at a bend angle of 31° which is compared to the asymmetric layouts in table 5.9.

Table 5 9: Head loss comparison for different layouts

Head Loss	Asymmetric Layout 1	Asymmetric Layout 2	Symmetric Layout (31° bend)
Outlet 1 (mm)	214.70	234.03	228.37
Outlet 2 (mm)	624.38	265.53	176.77

The value of head loss has significantly decreased with the introduction of bend in the inlet pipe to deviate the flow direction and by the use of symmetric bifurcation. A more significant drop in head loss is observed at outlet 2 which has decreased by 71.68% compared to asymmetric layout 1 and by 33.4% compared to asymmetric layout 2.

CHAPTER SIX: CONCLUSION AND RECOMMENDATION

6.1 Conclusion

The following conclusions are derived from this study:

i) The CFD analysis has been conducted for asymmetric and symmetric bifurcation layouts by developing the models in ANSYS SpaceClaim and performing analysis in Fluent Platform. Flow parameters such as pressure, velocity, mass flow rate has been computed using the surface integral function of ANSYS and these values have been used for subsequent calculations.

ii) The symmetric bifurcation layout, having a bend just upstream of the bifurcation, was successively revised by changing the bend angle by 1° in each revision, ranging the bend angle from 24° to 32°. CFD analysis was conducted on each of the layout to determine flow parameters (pressure, velocity, mass flow rate).

iii) The pressure field and velocity field for each layout were visualized by plotting the pressure distribution and velocity distribution in the mid plane of symmetry. Low pressure and low velocity region were observed at same location towards outlet 2 in the asymmetric layout 1 which signified the larger extent of head loss in that particular layout in a particular outlet. Similar phenomenon but with lesser intensity was observed in asymmetric layout 2. The pressure and velocity distributions were more or less uniform in the symmetric layouts. While changing the bend angle, the pressure and velocity distribution diagrams were not easily visually distinct from one bend angle to another. A high pressure and low velocity zone was observed at the crotch of the bifurcation for all layouts.

iv) The head loss for the two outlets in each layout was calculated. For outlet 1, the lowest value of head loss was obtained in asymmetric layout 1 i.e. 214.70 mm. In Asymmetric layout 2, that value is 234.03 mm and in the symmetric layout, the head loss at outlet 1 varied with the change in bend angle. The head loss decreased with increase in bend angle and the lowest value obtained at a bend angle of 32° was 223.3mm. For outlet 2, head loss was highest in the asymmetric layout 1 i.e. 624.38 mm. In Asymmetric Layout 2, that value

was 265.53mm and in the symmetric layout, head loss for outlet 2 increased with increase in bend angle, and the lowest value was 171.08mm at a bend angle of 24°.

6.2 Recommendations

i) The actual flow behavior can be more precisely predicted by incorporating the sickle plate in the design.

ii) More variations in the layout as well as in the geometry can be studied to achieve an optimum layout.

iii) Financial analysis of the different bifurcations can be carried out to determine the economic effect of incorporating bend in the main inlet pipe.

iv) Experimental verification of the results of at least one of the layouts can give a clearer confirmation of the whole simulation process.

REFERENCES

AEPC. (2014). *Guidelines for Detailed Feasibility Studies of Mini Hydropower Projects* (Issue June).

Aguirre, C. A., & Camacho, R. G. R. (2014). *Head Losses Analysis in Symmetrical Trifurcations of Penstocks - High Pressure Pipeline Systems CFD*. *2*(15), 24–27.

Ahmed, S. (1965). *Head Loss in Symmetrical Bifurcations*.

Anderson, J. D. (1992). Governing Equations of Fluid Dynamics. *Computational Fluid Dynamics*, 15–51. https://doi.org/10.1007/978-3-662-11350-9_2

ANSYS Inc. (2016). ANSYS Fluent Theory Guide v17.1. *ANSYS 17.1 Documentation*, *15317*(April), 850.

BIS. (2009). *Penstock Branch Design Manual* (Vol. 14, Issue November).

Casartelli, E., & Ledergerber, N. (2006). *Aspects of the Numerical Simulation for the Flow in Penstocks*. *1999*(December), 1–6.

Dangi, B., Bajracharya, T. R., & Timilsina, A. B. (2022). *Numerical Analysis of Manifold : A Case Study of Phukot Karnali Hydroelectric Project*. *July*.

Dhungana, S. (2020). *Flow analysis in eccentric bucket of Micro Pelton turbine: Multiphase modelling with transient state condition*. *2507*(February), 1–9.

Gisselbrecht, M., & Plaut, E. (2017). *High Reynolds number K - epsilon model of turbulent pipe flows with standard wall laws : first quantitative results*.

Hanumanthappa, M. S., Ali, R., Paswan, S., Chaphalkar, S. G., & Govindan, S. (2010). *Performance Evaluation of an Underground Penstock Bifurcation A Case Study*. 4–7.

Kandel, B., & Luitel, M. C. (2019). Computational Fluid Dynamics Analysis of Penstock Branching in Hydropower Project. *Journal of Advanced College of Engineering and Management*, *5*, 37–43. https://doi.org/10.3126/jacem.v5i0.26676

Koirala, R., Chitrakar, S., Neopane, H. P., Chhetri, B., & Thapa, B. (2017). Computational Design of Bifurcation: A Case Study of Darundi Khola Hydropower Project Ravi. *International Journal of Fluid Machinery and Systems*, *10*(1), 1–8. https://doi.org/10.5293/IJFMS.2017.10.1.001

Malik, R. K., & Paudel, P. (1970). 3D Flow Modeling of the First Trifurcation Made in Nepal. *Hydro Nepal: Journal of Water, Energy and Environment*, *5*(January), 56–61. https://doi.org/10.3126/hn.v5i0.2493

Miller, D. S. (1990). *Internal Flow Systems 2nd Edition*.

NEA. (2020). *Nepal Electricity Authority Annual Report 2019/20* (Vol. 1999, Issue December).

Parajuli, P., Satyal, S., Sigdel, S., & Karki, S. (2021). *Design Optimization of Internal Reinforced Bifurcation Using Fluid Structure Interaction (FSI) Technique, A Case Study of Maibeni Project Illam 9.51 MW* (Issue January).

Rajput, R. K. (1998). *A Textbook of Fluid Mechanics and Hydraulic Machines*.

Shaheed, R., Mohammadian, A., & Kheirkhah Gildeh, H. (2019). A comparison of standard k–ε and realizable k–ε turbulence models in curved and confluent channels. *Environmental Fluid Mechanics*, *19*(2), 543–568. https://doi.org/10.1007/s10652-018-9637-1

Sukhapure, M. K., Burns, M. A., Mahmud, M. T., & Spooner, M. J. (2017). CFD Modelling and Validation of Pipe Bifurcations. *13th International Conference on Heat Transfer, Fluid Mechanics and Thermodynamics*, 489–495.

Thapa, D., Chandra Luintel, M., & Ratna Bajracharaya, T. (2016). *Flow Analysis and Structural Design of Penstock Bifurcation of Kulekhani III HEP*. *May*, 271–276.

Versteeg, H. K., & Malalasekera, W. (2005). An Introduction to Computational Fluid Dynamics. In *IEEE Concurrency* (Vol. 6, Issue 4). https://doi.org/10.1109/mcc.1998.736434

State, Kerala, and Electricity Board. (2017) *Computational Fluid Dynamics (CFD) Analysis of Bifurcation*, November.

J. H. Bambei, 2012, "*Steel Penstock*," Ed. 1 ASCE Publications.

ASCE, 2001, *Steel Penstocks*

APPENDIX A: 2D DRAWINGS OF SYMMETRIC LAYOUTS FOR VARIED BEND ANGLE

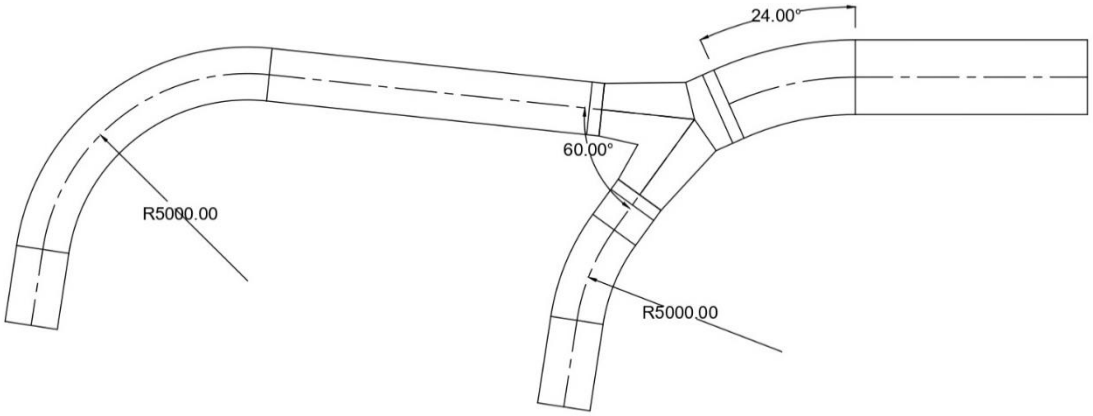

Figure A1: Symmetric Layout with bend angle 24°

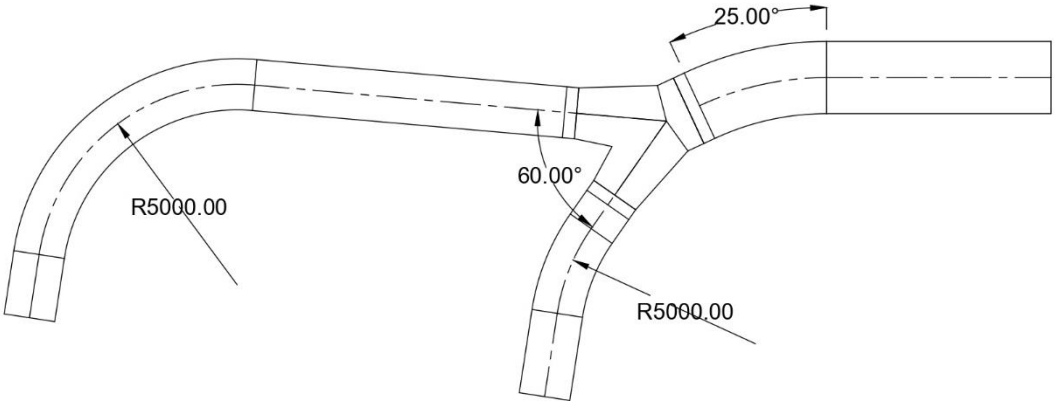

Figure A2: Symmetric Layout with bend angle 25°

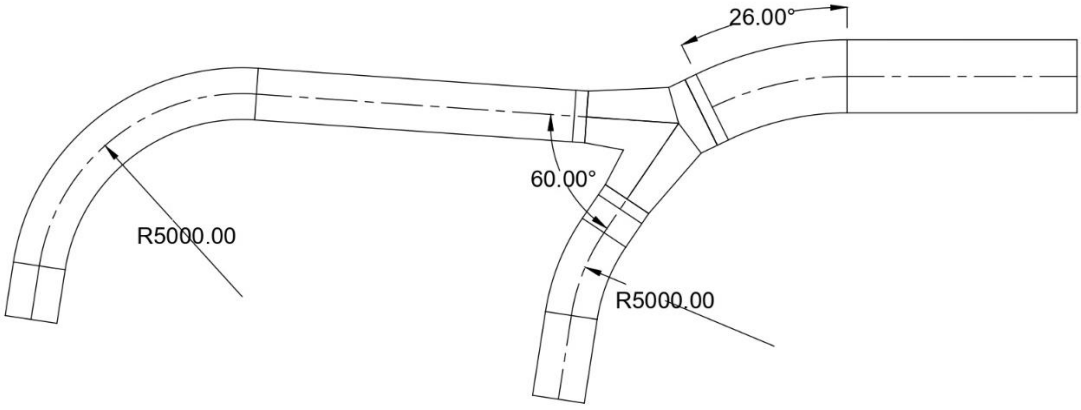

Figure A3: Symmetric Layout with bend angle 26°

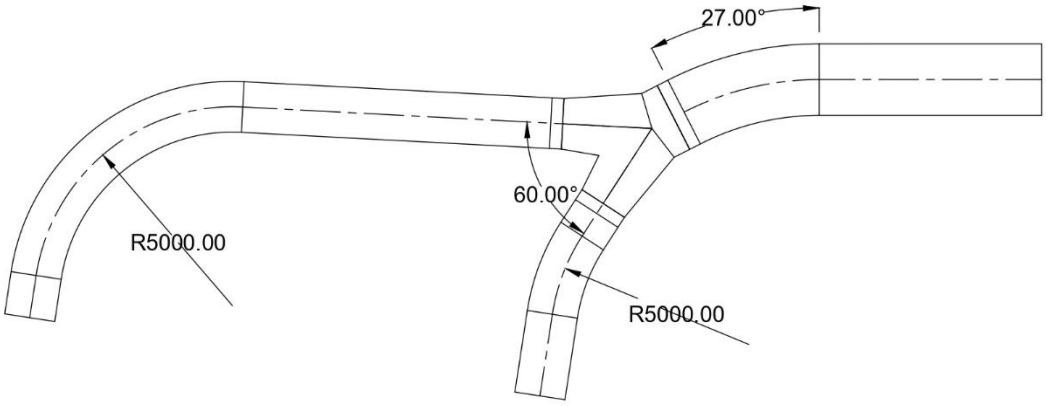

Figure A4: Symmetric Layout with bend angle 27°

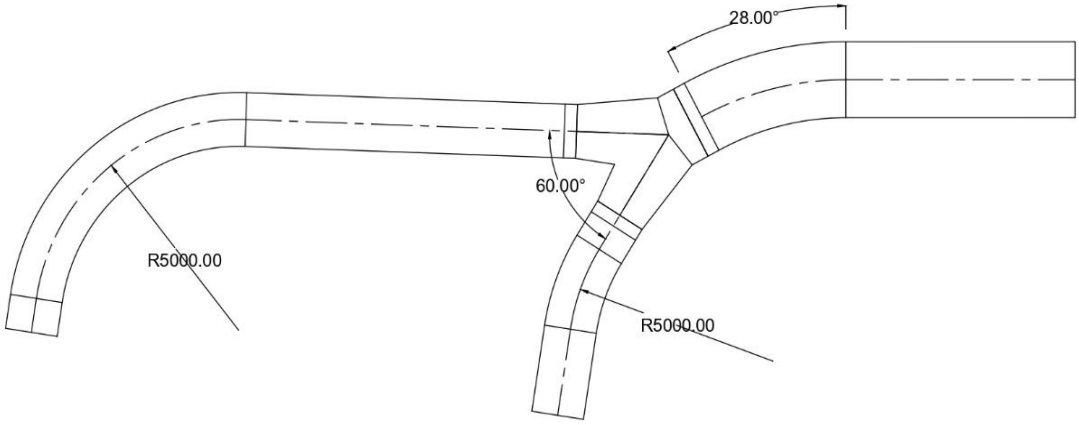

Figure A5: Symmetric Layout with bend angle 28°

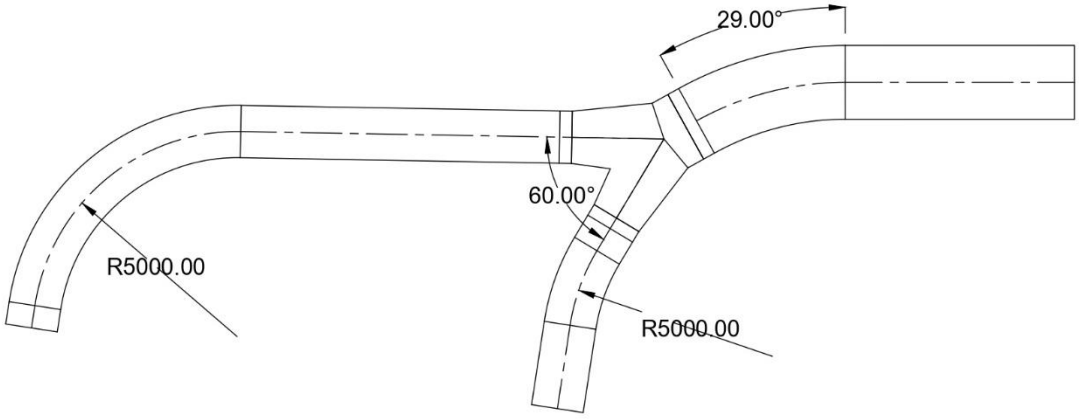

Figure A6: Symmetric Layout with bend angle 29°

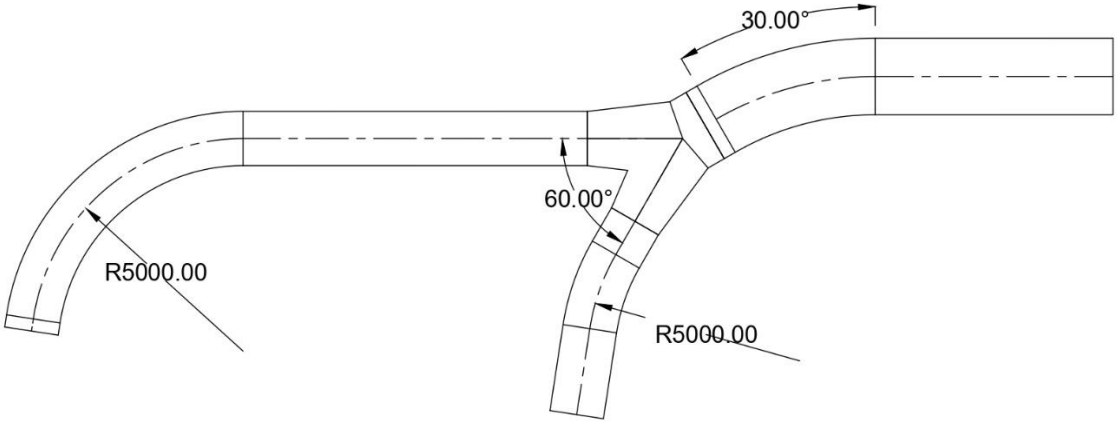

Figure A7: Symmetric Layout with bend angle 30°

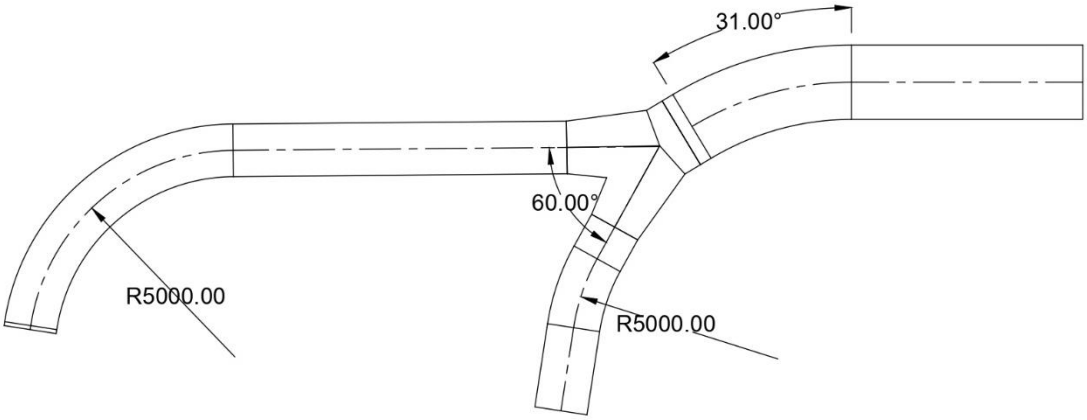

Figure A8: Symmetric Layout with bend angle 31°

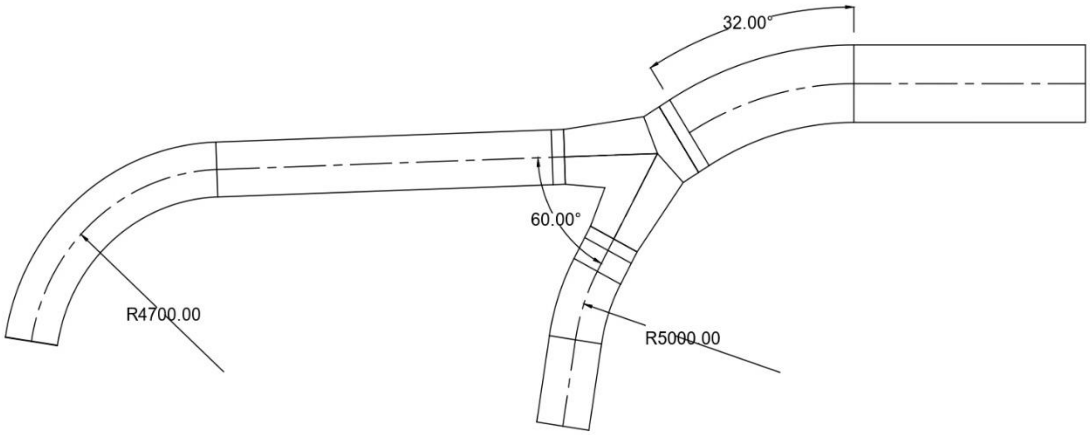

Figure A9: Symmetric Layout with bend angle 32°

APPENDIX B: PRESSURE CONTOURS ON SYMMETRIC LAYOUTS FOR VARIED BEND ANGLES

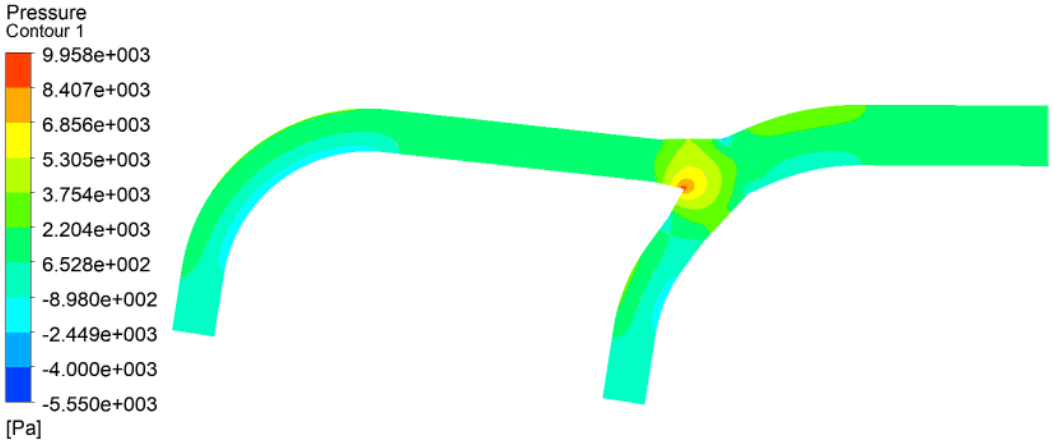

Figure B1: Pressure Contour (Bend angle 24°)

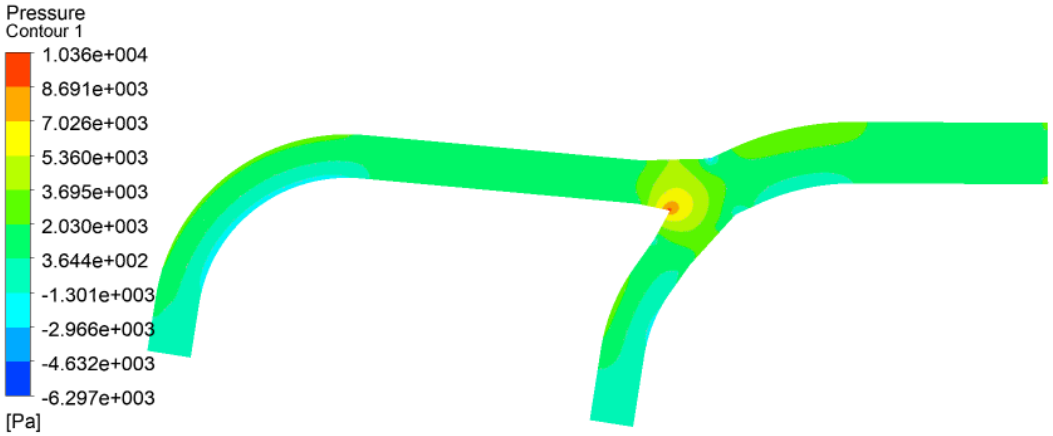

Figure B2: Pressure Contour (Bend angle 25°)

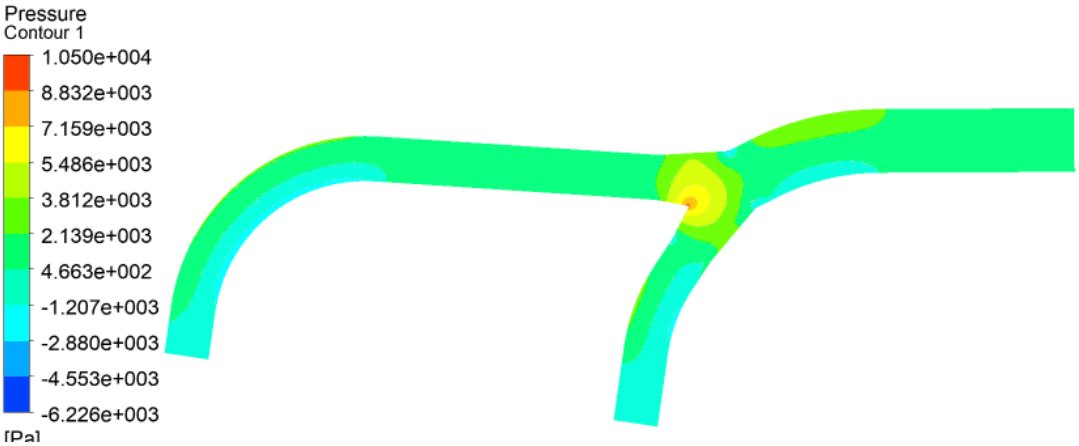

Figure B3: Pressure Contour (Bend angle 26°)

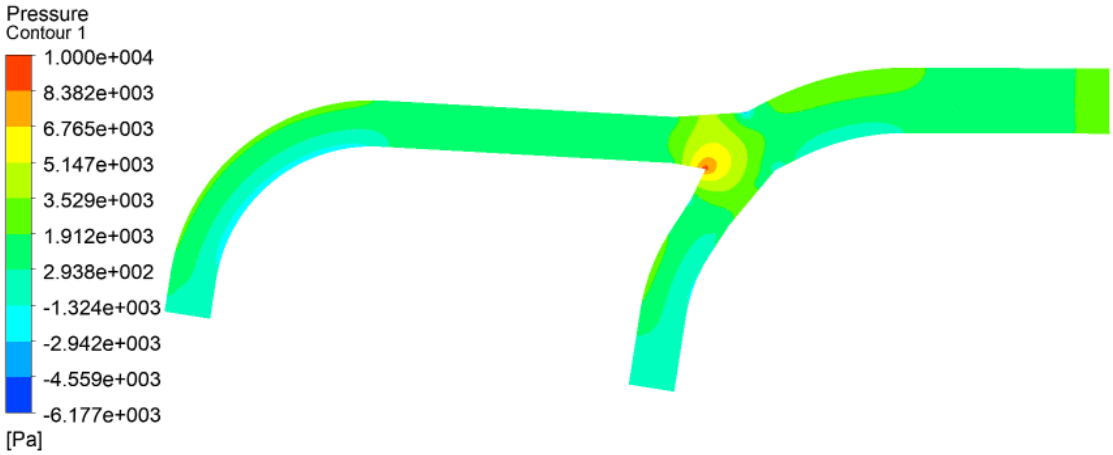

Figure B4: Pressure Contour (Bend angle 27°)

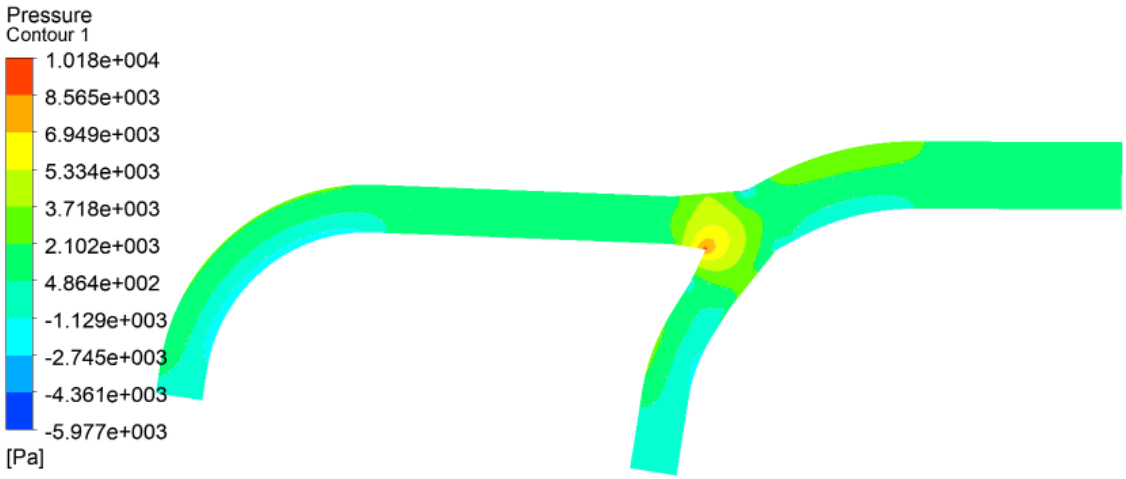

Figure B5: Pressure Contour (Bend angle 28°)

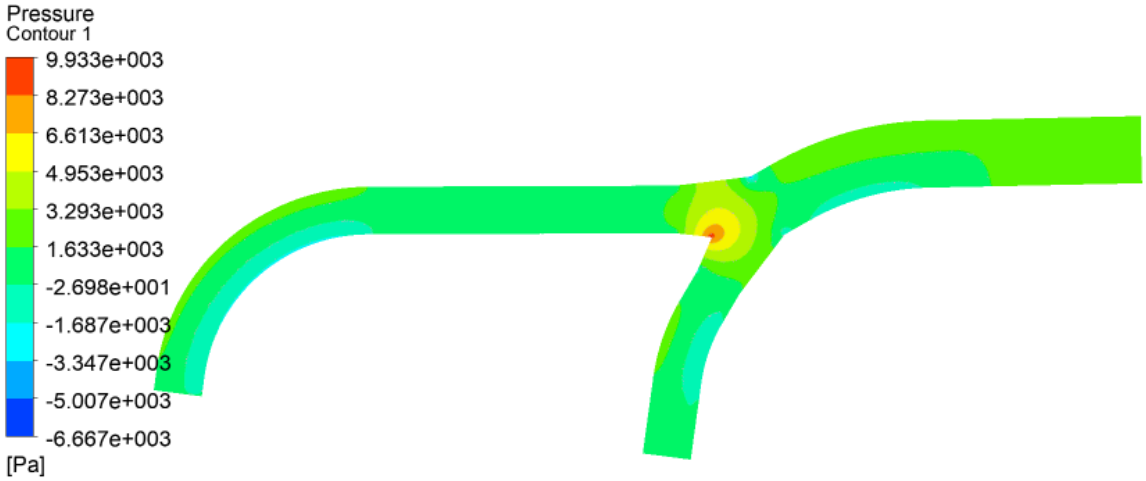

Figure B6: Pressure Contour (Bend angle 29°)

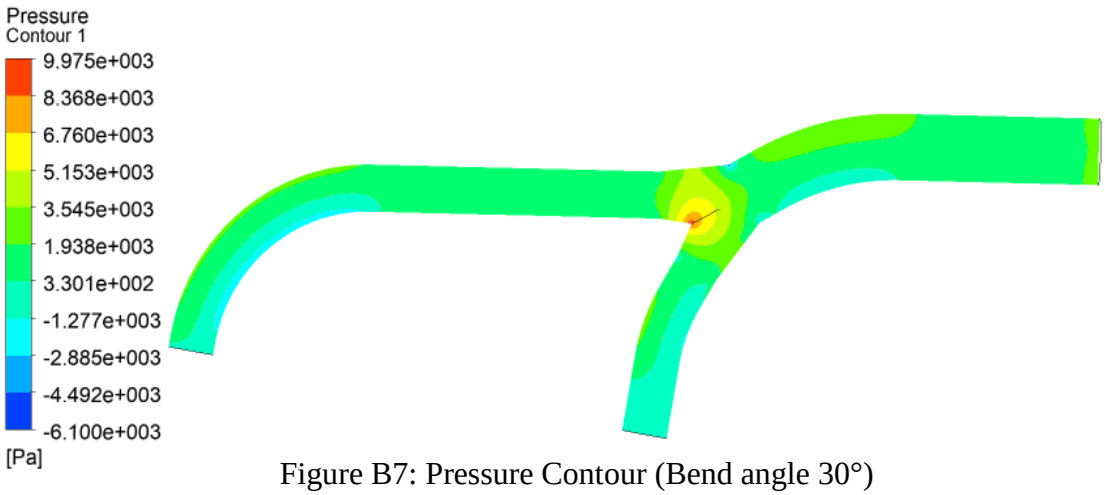

Figure B7: Pressure Contour (Bend angle 30°)

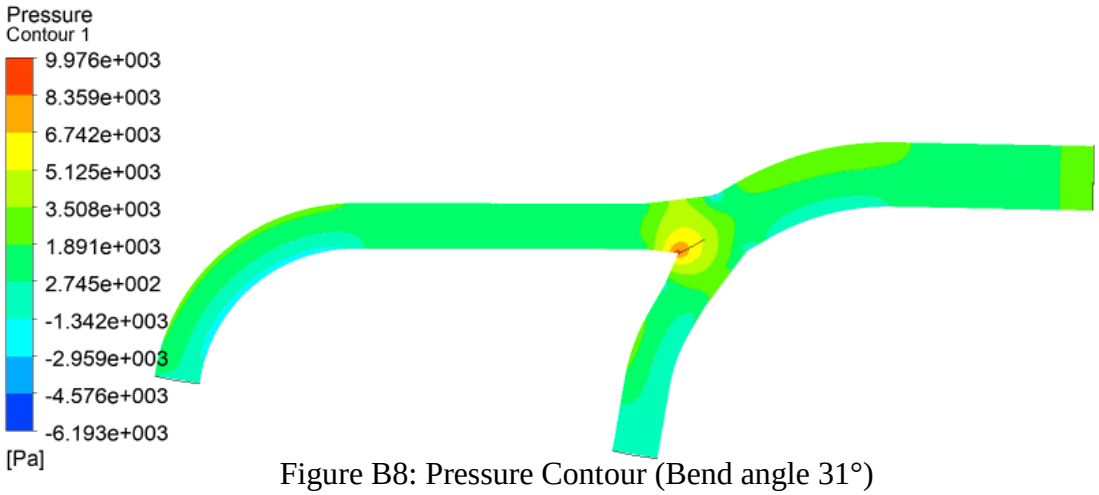

Figure B8: Pressure Contour (Bend angle 31°)

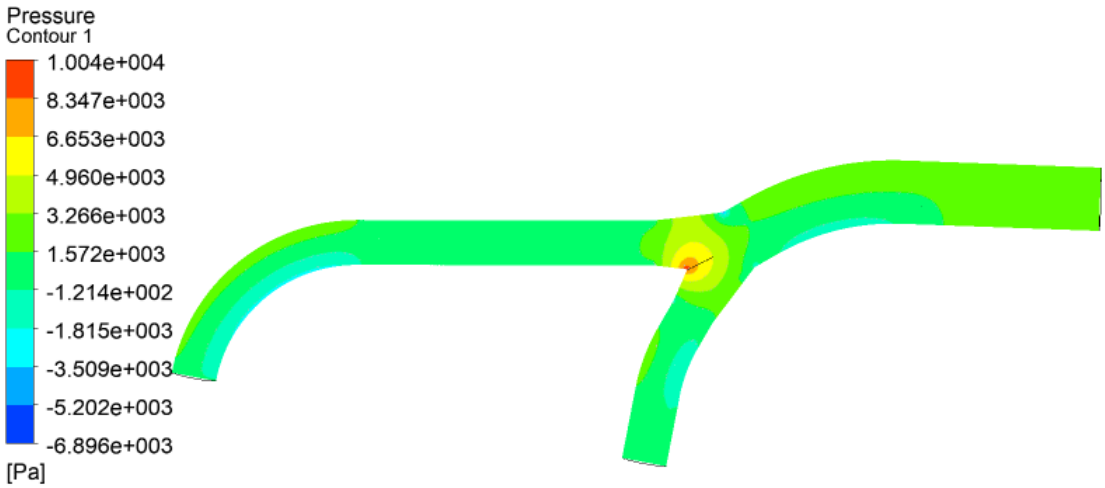

Figure B9: Pressure Contour (Bend angle 32°)

APPENDIX C: VELOCITY CONTOURS ON SYMMETRIC LAYOUTS FOR VARIED BEND ANGLES

Figure C1: Velocity Contour (Bend angle 24°)

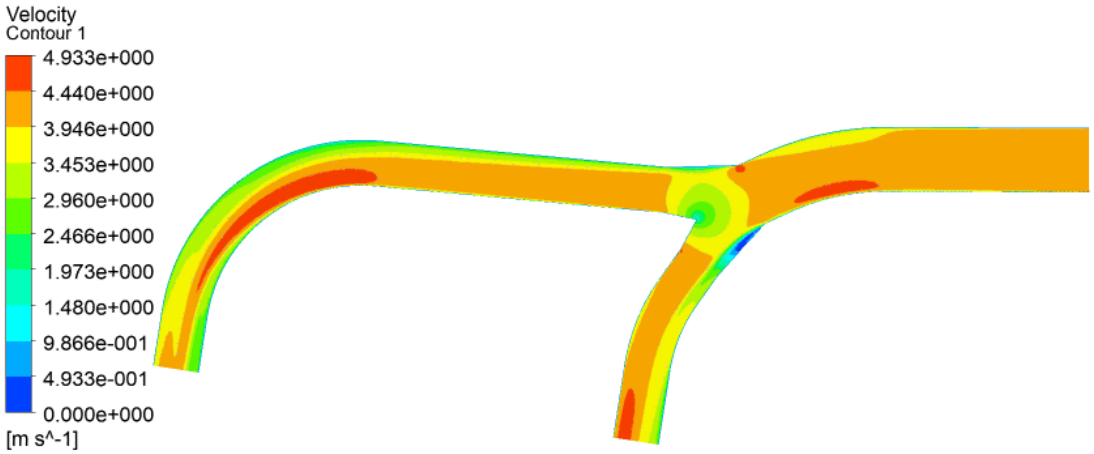

Figure C2: Velocity Contour (Bend angle 25°)

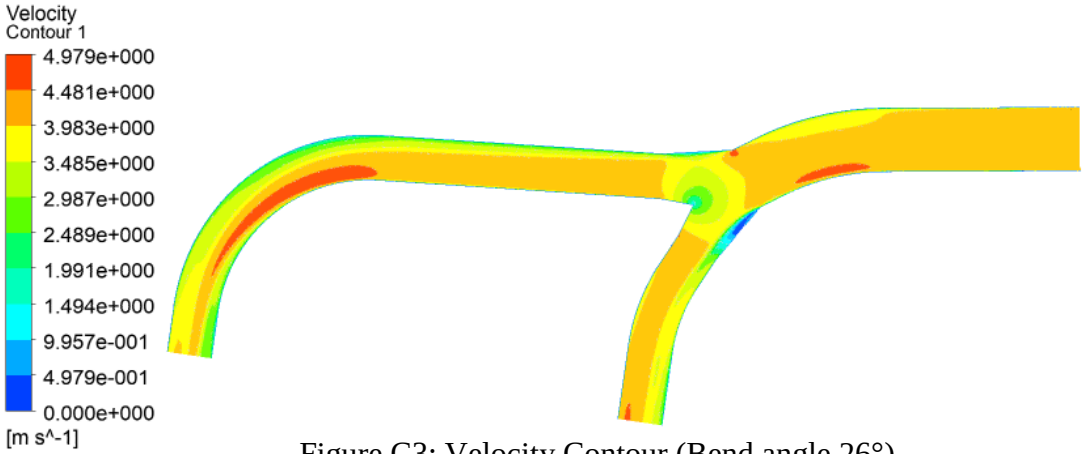

Figure C3: Velocity Contour (Bend angle 26°)

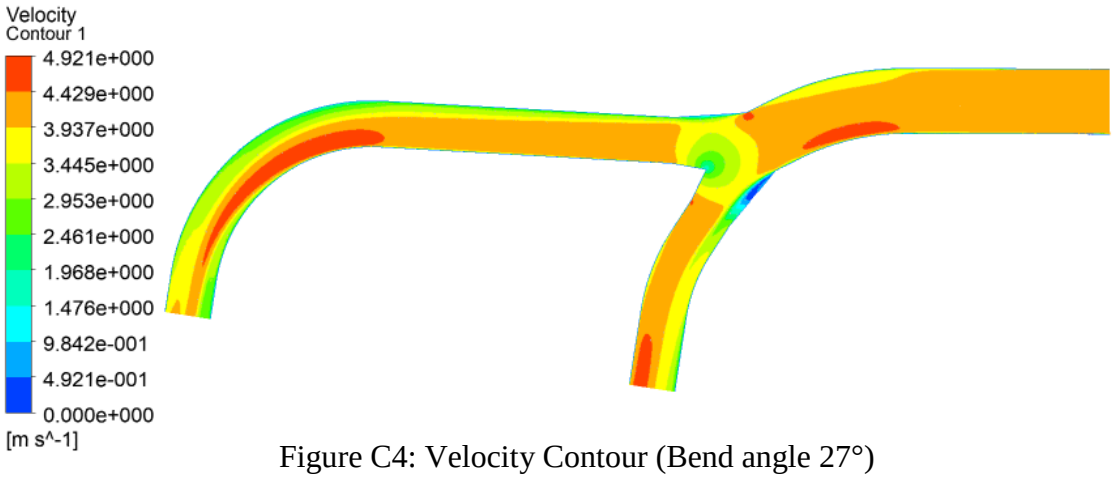

Figure C4: Velocity Contour (Bend angle 27°)

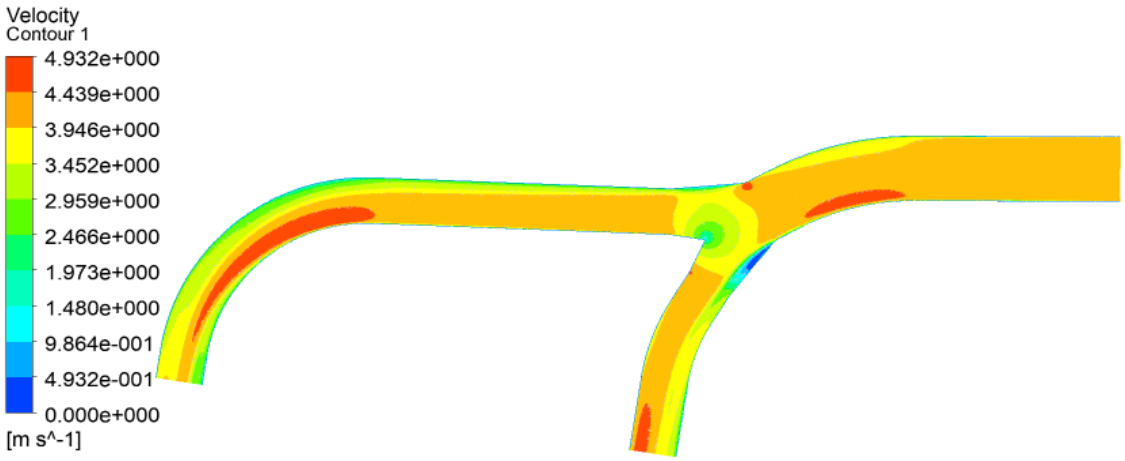

Figure C5: Velocity Contour (Bend angle 28°)

Figure C6: Velocity Contour (Bend angle 29°)

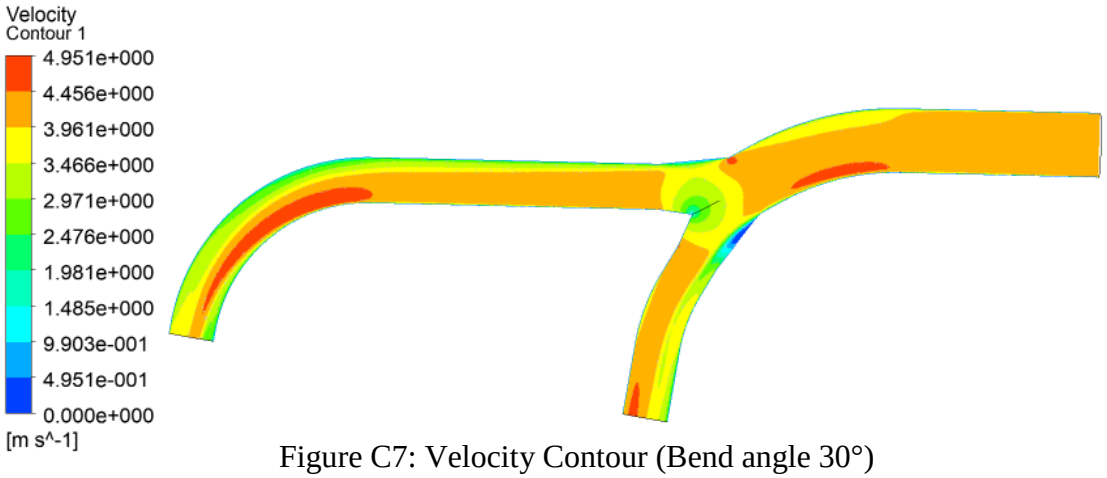

Figure C7: Velocity Contour (Bend angle 30°)

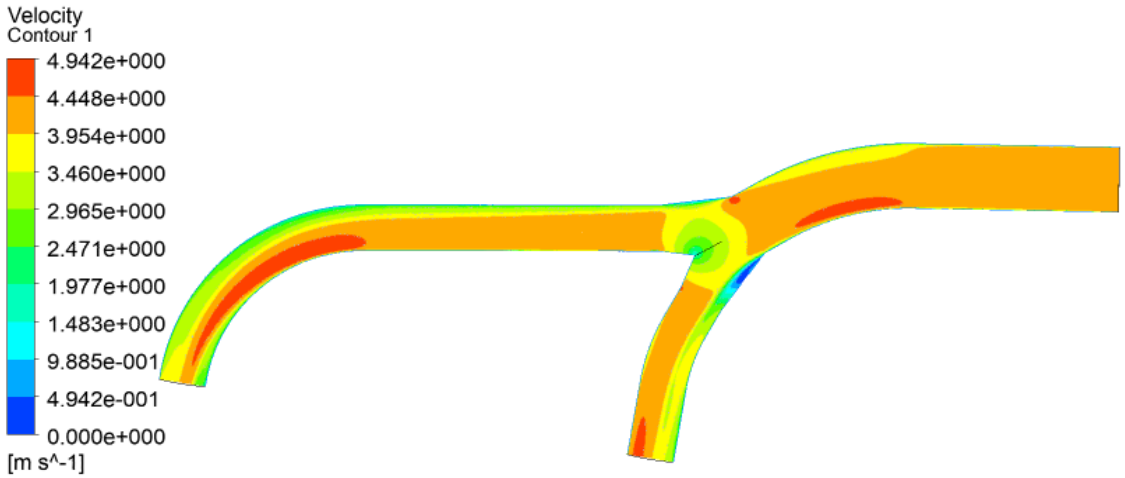

Figure C8: Velocity Contour (Bend angle 31°)

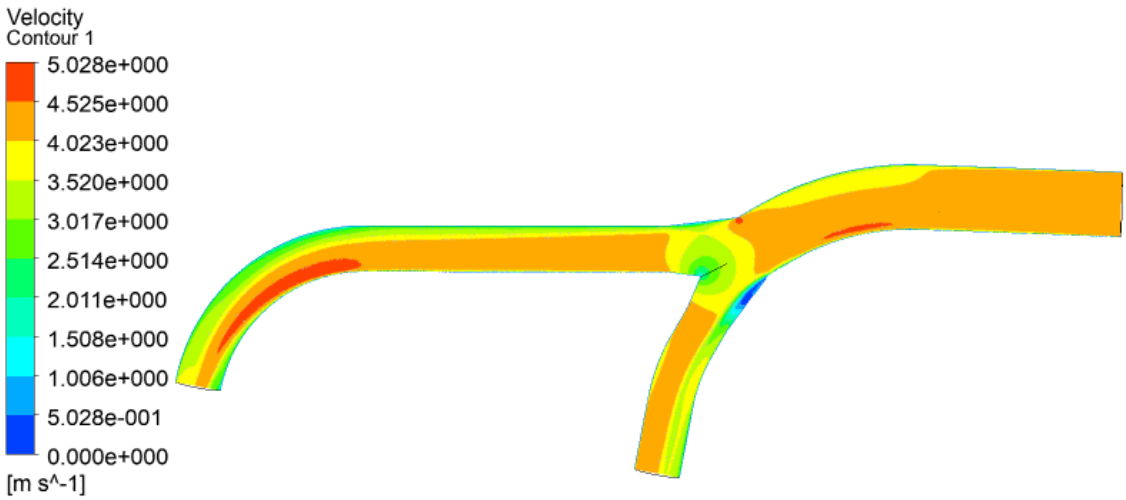

Figure C9: Velocity Contour (Bend angle 32°)

APPENDIX D: TURBULENT KINETIC ENERGY CONTOURS ON SYMMETRIC LAYOUTS FOR VARIED BEND ANGLES

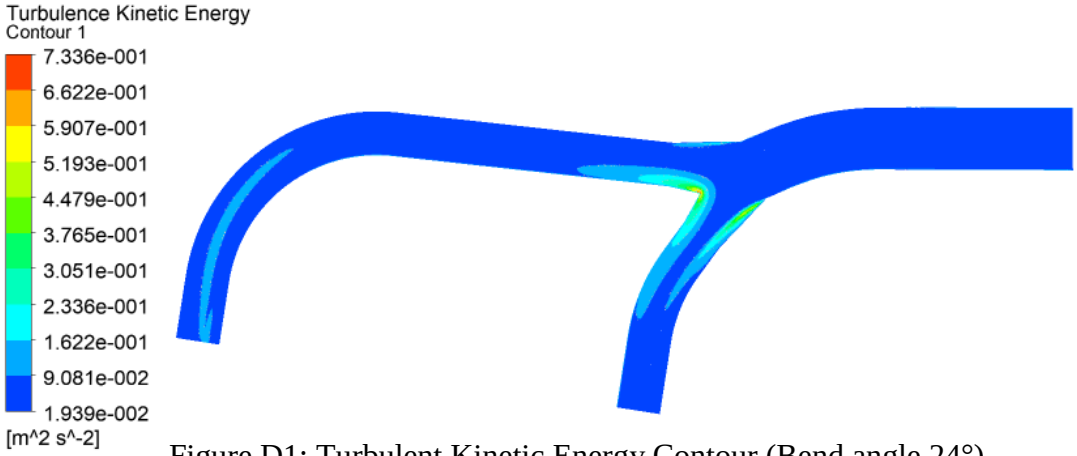

Figure D1: Turbulent Kinetic Energy Contour (Bend angle 24°)

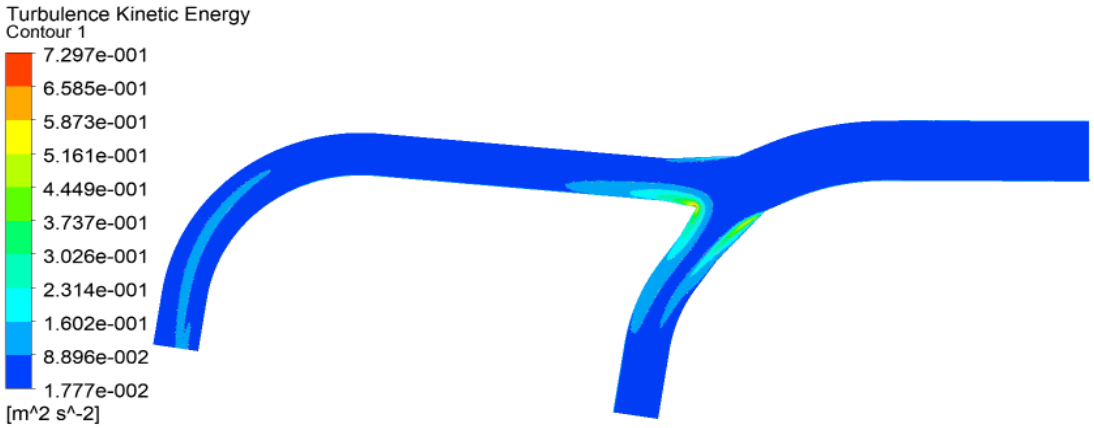

Figure D2: Turbulent Kinetic Energy Contour (Bend angle 25°)

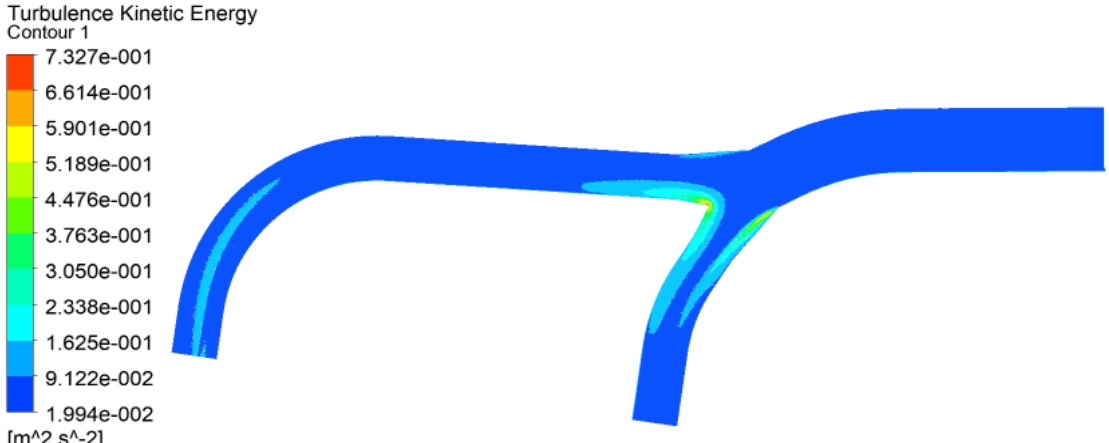

Figure D3: Turbulent Kinetic Energy Contour (Bend angle 26°)

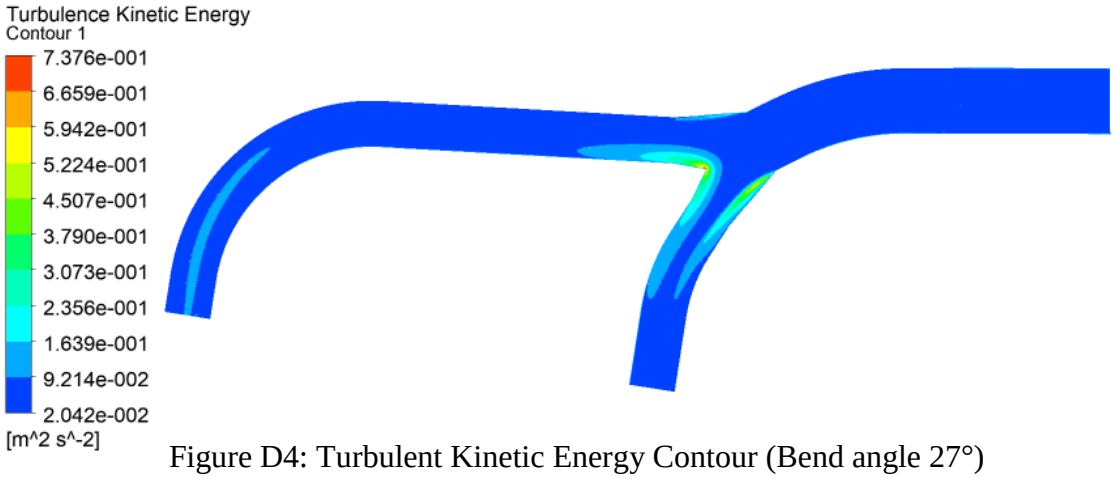

Figure D4: Turbulent Kinetic Energy Contour (Bend angle 27°)

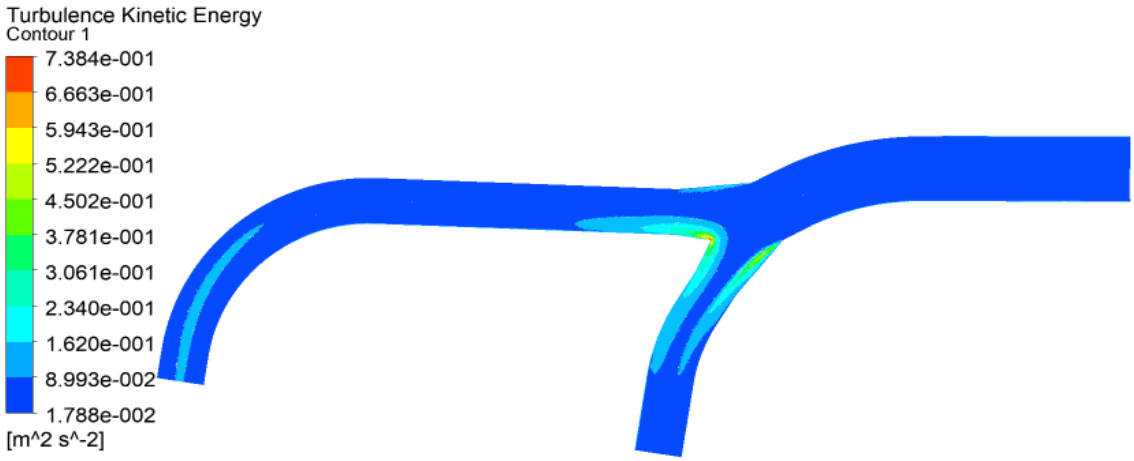

Figure D5: Turbulent Kinetic Energy Contour (Bend angle 28°)

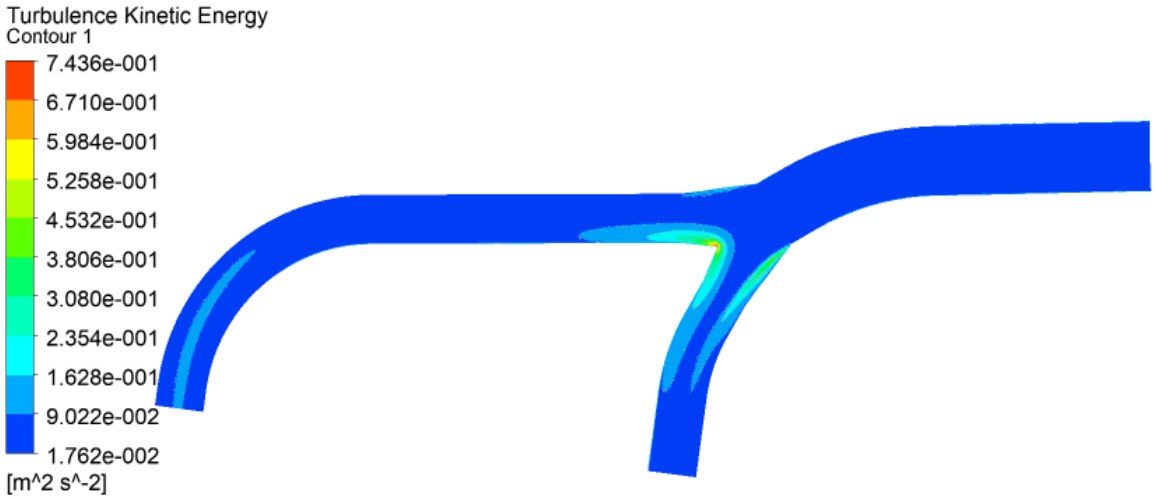

Figure D6: Turbulent Kinetic Energy Contour (Bend angle 29°)

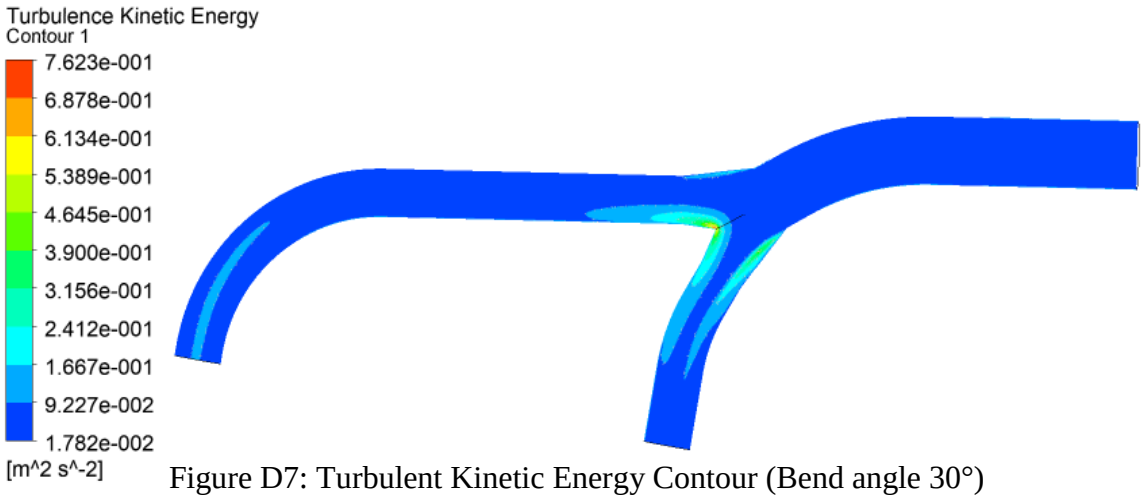

Figure D7: Turbulent Kinetic Energy Contour (Bend angle 30°)

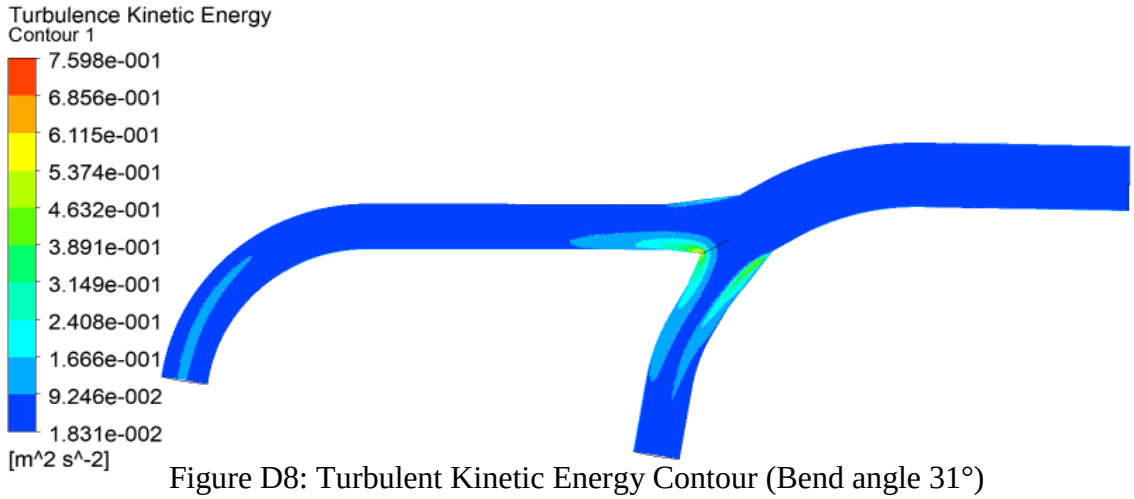

Figure D8: Turbulent Kinetic Energy Contour (Bend angle 31°)

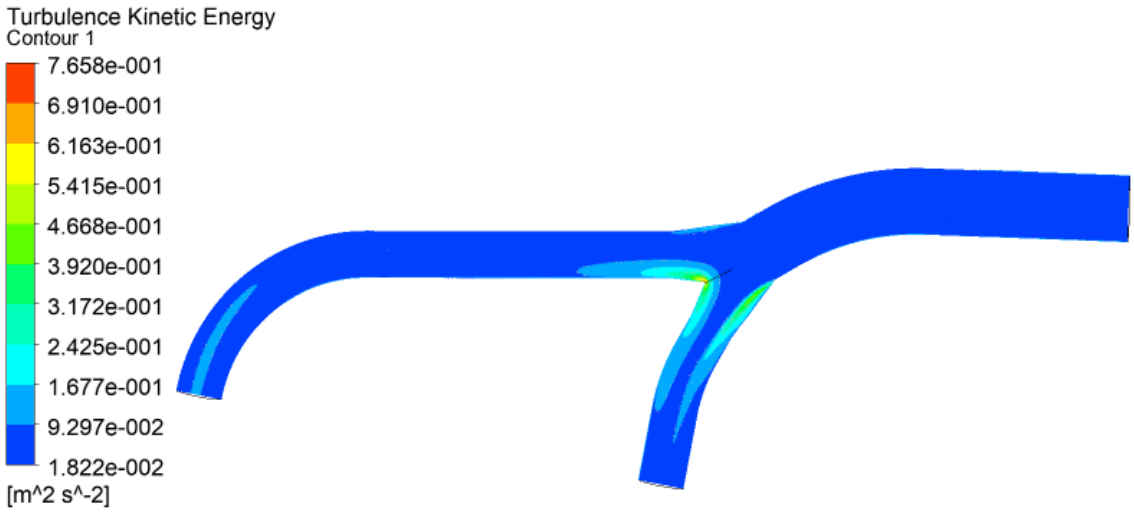

Figure D9: Turbulent Kinetic Energy Contour (Bend angle 32°)

APPENDIX E: MOODY DIAGRAM

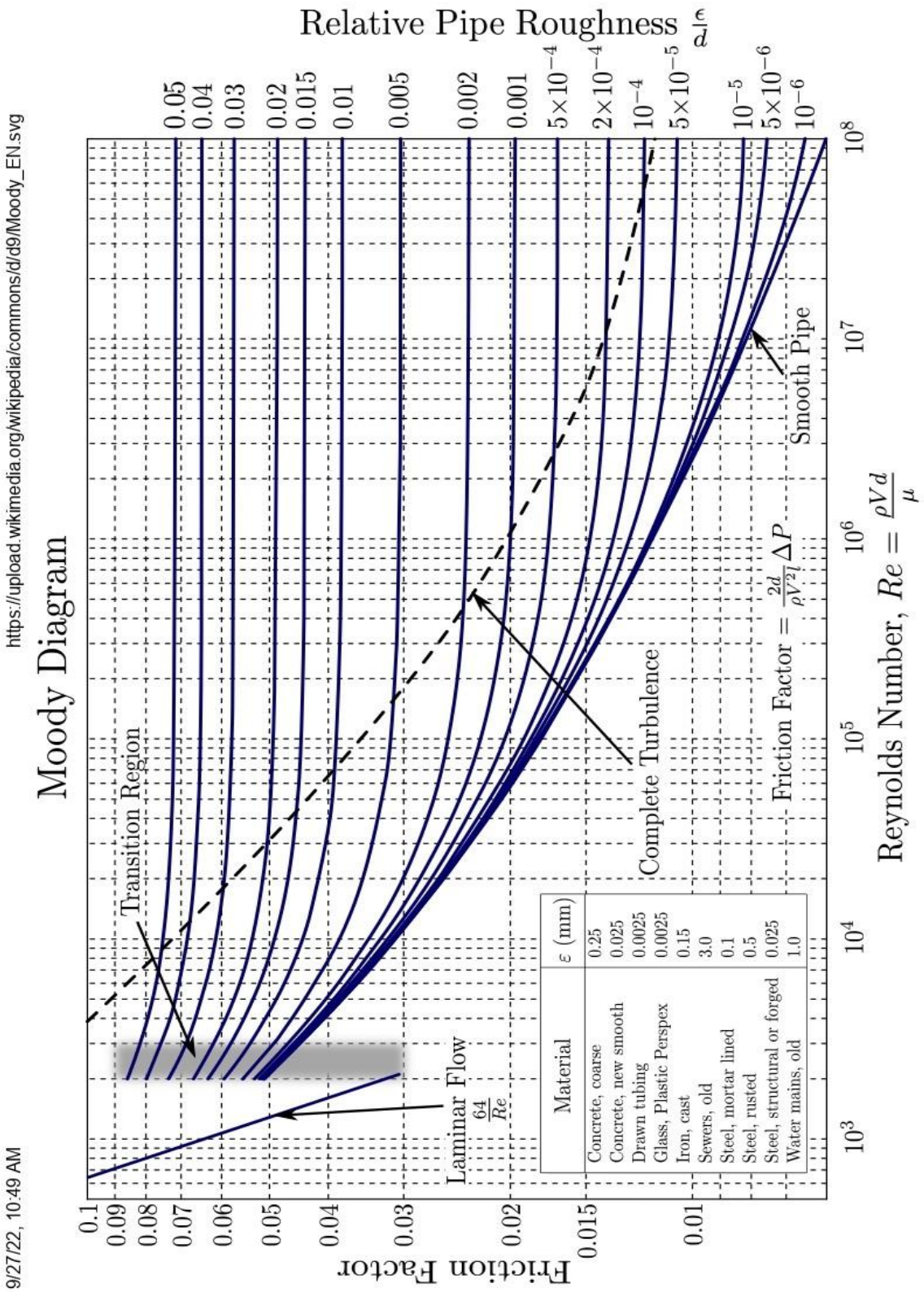

https://upload.wikimedia.org/wikipedia/commons/d/d9/Moody_EN.svg

9/27/22, 10:49 AM